

**COPLANAR WAVEGUIDE-BASED LOW PASS FILTER DESIGN WITH
NON-UNIFORM SIGNAL TRACE AND GROUND PLANES USING
DIFFERENT OPTIMIZATION ALGORITHMS**

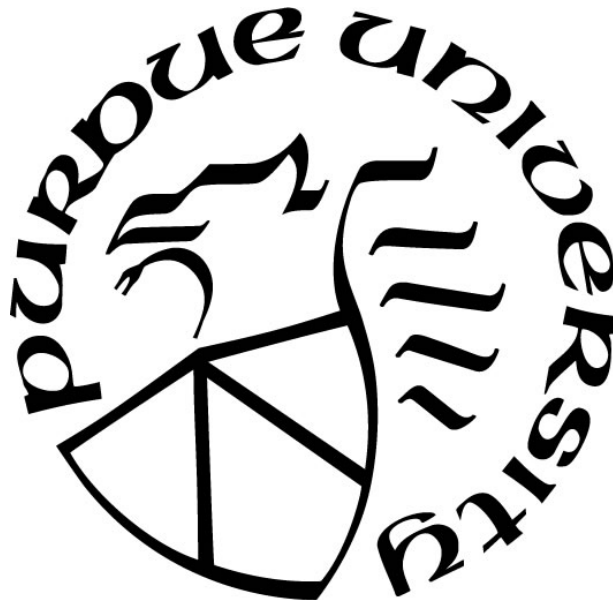
by
Qizhen Li

A Thesis

Submitted to the Faculty of Purdue University

In Partial Fulfillment of the Requirements for the degree of

Master of Science in Electrical and Computer Engineering



School of Electrical & Computer Engineering

Hammond, Indiana

May 2019

THE PURDUE UNIVERSITY GRADUATE SCHOOL
STATEMENT OF COMMITTEE APPROVAL

Dr. Khair Al Shamaileh, Chair

Department of Electrical and Computer Engineering

Dr. Vijay Devabhaktuni, Co-Chair

Department of Electrical and Computer Engineering

Dr. Quamar Niyaz

Department of Electrical and Computer Engineering

Dr. Lucy Yang

Department of Electrical and Computer Engineering

Approved by:

Dr. Vijay Devabhaktuni

Head of the Graduate Program

This thesis is dedicated to the memory of my respectable grandfather

ACKNOWLEDGMENTS

I would like to express my profound acknowledgment and appreciation to my thesis advisor Prof. Khair Al Shamaileh for his great help, patience, encouragement, guidance throughout my graduate career.

Besides, I would like to thank my parents for supporting me in studying abroad and giving me consistent encouragement.

TABLE OF CONTENTS

LIST OF TABLES	7
LIST OF FIGURES	8
ABSTRACT	10
CHAPTER 1. INTRODUCTION	11
1.1 Microwave Theory	11
1.2 Coplanar Waveguide (CPW)	11
1.3 Filters	12
1.4 Motivation of the Study	13
1.5 Thesis Scope	13
CHAPTER 2. LITERATURE SURVEY	14
CHAPTER 3. PROPOSED CB-CPW-BASED LPF DESIGNS.....	17
3.1 Structural Designs	17
3.1.1 Type 1: CB-CPW with Varied Signal Trace and Constant Gap-to-trace Separation	17
3.1.2 Type 2: CB-CPW with Varied Signal Trace and Varied Gap-to-trace Separation ...	18
3.1.3 Type 3: CB-CPW with Varied Signal Trace and Fixed Ground-to-ground Gap	19
3.2 Mathematical Methodology	19
3.3 Analytical Results	22
3.3.1 Type 1	23
A. Trust-region-reflective Algorithm	23
B. Genetic Algorithm	23
C. Particle Swarm Optimization Algorithm	24
3.3.2 Type 2	25
A. Trust-region-reflective Algorithm	25
B. Genetic Algorithm	26
C. Particle Swarm Optimization Algorithm	27
3.3.3 Type 3	28
A. Trust-region-reflective Algorithm	28
B. Genetic Algorithm	29

C. Particle Swarm Optimization Algorithm	30
3.3.4 Comparison between Three Algorithms	32
3.3.5 Comparison between Three Proposed Types of Structures	34
3.4 Simulated Results.....	35
3.4.1 Simulated Results of the Three Types of the CB-CPW LPF.....	40
3.4.2 Comparison between Analytical and Simulated Results	42
3.4.3 Design of the Conventional Stepped-impedance CB-CPW LPF	44
3.4.4 Comparison between Conventional and Proposed Non-uniform CB-CPW LPFs	47
CHAPTER 4. Proposed conventional CPW-based LPF	49
4.1 Analytical Results	49
4.2 Simulated Results.....	50
CHAPTER 5. CONCLUSIONS.....	51
REFERENCES	52

LIST OF TABLES

Table 1	Type 1 Optimized Fourier Series Coefficients	31
Table 2	Type 2 Optimized Fourier Series Coefficients	32
Table 3	Type 3 Optimized Fourier Series Coefficients	32
Table 4	Comparison between the Three Algorithms on Type 1	33
Table 5	Comparison between the Three Algorithms on Type 2	33
Table 6	Comparison between the Three Algorithms on Type 3	33
Table 7	Relevant Parameters of the Designed Stepped-Impedance CB-CPW LPF	45

LIST OF FIGURES

Figure 1 Cross Section of a Conventional CPW Structure	12
Figure 2 CB-CPW Geometry.....	12
Figure 3 Top View of Type 1 Structure.....	17
Figure 4 Top View of Type 2 Structure.....	18
Figure 5 Top View of Type 3 Structure.....	19
Figure 6 Type 1 Optimized Width Profile Using TRRA with Corresponding Analytical Response	23
Figure 7 Type 1 Optimized Width Profile Using GA with Corresponding Analytical Response	24
Figure 8 Type 1 Optimized Width Profile Using PSO with Corresponding Analytical Response	25
Figure 9 Type 2 Optimized Width Profile Using TRRA with Corresponding Analytical Response	26
Figure 10 Type 2 Optimized Width Profile Using GA with Corresponding Analytical Response	27
Figure 11 Type 2 Optimized Width Profile Using PSO with Corresponding Analytical Response	28
Figure 12 Type 3 Optimized Width Profile Using TRRA with Corresponding Analytical Response	29
Figure 13 Type 3 Optimized Width Profile Using GA with Corresponding Analytical Response	30
Figure 14 Type 3 Optimized Width Profile Using PSO with Corresponding Analytical Response	31
Figure 15 Type 1 Comparison of Analytical Results between Three Algorithms.....	33
Figure 16 Comparison of Analytical Results Using TRRA between Three Types of Designs ...	34
Figure 17 Schematic of the 3D model	35
Figure 18 Interface of Assigning Material.....	36
Figure 19 Interface of Assigning Boundary.....	36
Figure 20 Schematic of the Radiation Box	37

Figure 21 Schematic of the Excitation Surface.....	38
Figure 22 Screenshot of Simulation Setup.....	39
Figure 23 Adding Frequency Sweep.....	40
Figure 24 Type 1 CB-CPW LPF and Corresponding Simulated Results	41
Figure 25 Type 2 CB-CPW LPF and Corresponding Simulated Results	41
Figure 26 Type 3 CB-CPW LPF and Corresponding Simulated Results	42
Figure 27 Comparison between Analytical and Simulated Results on Type 1.....	43
Figure 28 Comparison between Analytical and Simulated Results on Type 2.....	43
Figure 29 Comparison between Analytical and Simulated Results on Type 3.....	44
Figure 30 Setting up Substrate.....	45
Figure 31 Schematic of the Designed Stepped-Impedance CB-CPW LPF Circuit.....	46
Figure 32 Simulated Results of 2D Designed Circuit.....	46
Figure 33 Designed Stepped-Impedance CB-CPW LPF and Corresponding Simulated Result	47
Figure 34 Simulated Results between Three Types of Designs and Conventional CB-CPW LPF.....	47
Figure 35 Optimized CPW LPF Width Profile with Corresponding Analytical Response.....	49
Figure 36 Optimized CPW LPF and Corresponding Simulated Results	50

ABSTRACT

Author: Li, Qizhen. MS

Institution: Purdue University

Degree Received: May 2019

Title: Coplanar Waveguide-based Low Pass Filter Design with Non-uniform Signal Trace and Ground Planes Using Different Optimization Algorithms

Committee Chair: Khair Al Shamaileh

In this study, a novel and systematic methodology for the design and optimization of conductor-backed coplanar waveguide (CB-CPW) based low pass filter (LPF) is proposed. The width of the signal trace is continuously varied using a truncated Fourier series, and the adjacent gaps are designed in several types established on a specific optimization setup to obtain predefined electrical characteristics with maximum compactness taking into account physical constraints. Trust-region-reflective algorithm (TRRA), genetic algorithm (GA), and particle swarm optimization algorithm (PSO) are taken into account to minimize the developed bound-constrained non-linear objective function respectively.

All types are programmed and analytically verified in MATLAB. Solutions include design parameters such as the physical length and width of the structure, which will be drawn in AutoCAD later on. Also, the optimized layouts are exported to Ansys High Frequency Structure Simulation (HFSS) software for simulation and validation. Non-uniform CB-CPW LPFs are optimized and simulated over a frequency range of 0-6 GHz with a cutoff frequency of 2 GHz. Simulation results show a good agreement with the analytical ones.

Keywords—conductor-backed coplanar waveguide (CB-CPW), low pass filter (LPF), trust-region-reflective algorithm (TRRA), genetic algorithm (GA), particle swarm optimization algorithm (PSO).

CHAPTER 1. INTRODUCTION

1.1 Microwave Theory

In microwave engineering, where frequencies extend from 300 MHz to 300 GHz (corresponding wavelengths from 1 mm to 1 m), the physical dimension of a circuit approaches the magnitude of the wavelength of the signal. Circuit design and construction are far more complicated as standard circuit theory cannot be used. Therefore, conventional lumped circuit elements such as inductance, capacitance, and resistance (i.e., *LRC*) fail to predict signal integrity and do not respond as expected at such high frequencies. To move signals from one port to another, conventional wires are replaced with other types of “guiding media”. As a result, distributed transmission lines such as microstrip lines and waveguides are utilized in high-frequency applications and microwave theory is utilized.

1.2 Coplanar Waveguide (CPW)

Transmission lines conduct alternating current of radio-frequency. In practice, there are mainly three types of planar transmission lines: 1) microstrip transmission lines, 2) striplines, and 3) coplanar waveguide (CPW). When choosing proper electromagnetic wave guiding transmission techniques, microstrip lines and striplines are generally considered due to the reasonable simplicity and ease of fabrication. However, conventional CPW technology, introduced in [1], or conductor-backed CPW (CB-CPW) technology [2] has more advantages, such as the low transmission losses and the convenient series and shunt mounting of passive and active devices without substrate drilling as well as reduced radiation and low dispersion [3,4].

Conventional CPW consists of a substrate having H thickness, with a relative permittivity ϵ_r , and a center conductor with a specific width W separated from a pair of adjacent ground planes with certain gap S , on the same plane on top of a dielectric material as shown in Figure 1. CB-CPW adds a ground plane to the bottom of the basic CPW circuit structure as shown in Figure 2, some are designed with plated through holes (PTHs) connecting the top and bottom ground planes [5]. And higher order mode suppression in CB-CPW structures using vias or shorting pins to connect the coplanar side grounds to the lower ground plane has been suggested in [6-10].

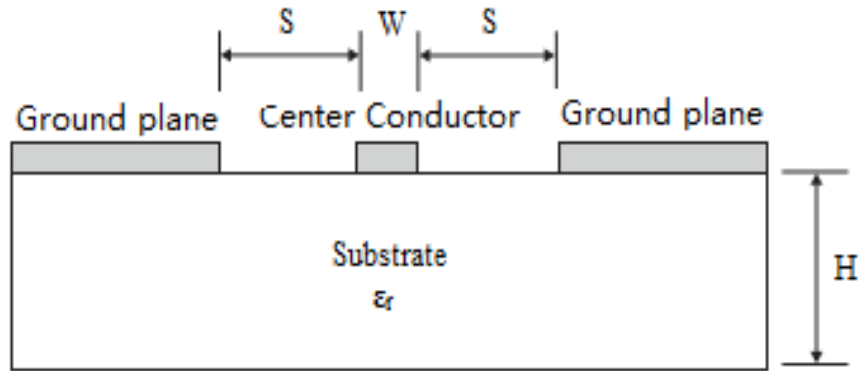


Figure 1 Cross Section of a Conventional CPW Structure

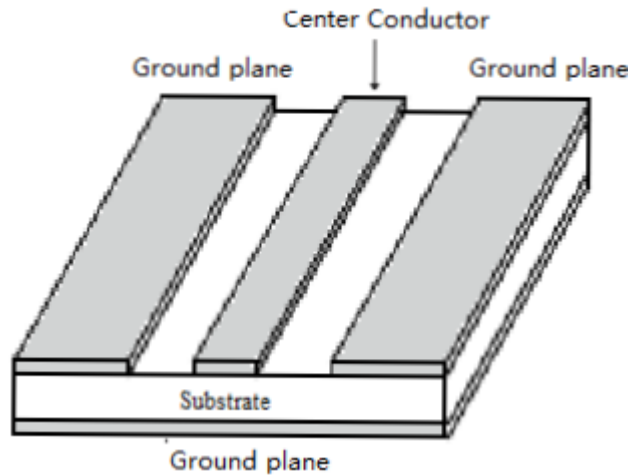


Figure 2 CB-CPW Geometry

The added ground plane in CB-CPW circuits provides additional mechanical stability compared to CPW circuits, with improved thermal management for higher-power circuits and devices. Moreover, the lower ground can be used for heat sinking purposes while providing mechanical support and preventing the fields from coupling to interconnects on lower circuit layers [11-13].

1.3 Filters

Filters also play a crucial role in modern communication circuitry. In general, a filter is a two-port network used to eliminate unwanted frequencies in a microwave system. And an ideal LPF is characterized by a unity power loss ratio in the passband region with infinite attenuation at

the stopband region. In other word, the transmission parameter, S_{21} , is supposed to be 0 dB within the passband and as small as possible in the stopband. LPFs have been extensively used to suppress undesired modes and spurious signals in nonlinear devices like mixers and frequency multipliers, etc. Also, they have been used to convert analog signals to band-limited signals before sampling and digitization.

1.4 Motivation of the Study

In spite of the fact that CPW technology has been highly considered, it has been found that there is still a lack of systematic methodologies which could successfully overcome the challenges of structural compactness, fabrication, complexity, and achieving an acceptable electrical performance. Accordingly, the proposed designs are developed for the purposes of creating optimal compact CPW-based LPFs with good manufacturability and optimum performance in accordance to S parameters under arbitrary given input conditions. All input parameters including substrate properties, transmission line dimensions and operating frequencies can be customized according to different demands.

1.5 Thesis Scope

In this study, a design of a CB-CPW LPF is proposed by modulating the width profiles of the center conductor and the adjacent ground planes. The width of the signal trace and adjacent grounds are varied along the propagation path of the electromagnetic (EM) wave, and are expressed as a truncated Fourier series expansion. The series coefficients are determined based on an optimization-driven procedure, where optimum frequency matching at the passband, end terminations (i.e., impedance matching), and the minimum-maximum signal trace widths are addressed in the optimization process. Besides, three algorithms are adopted and evaluated for an optimum performance. Comparisons are made among algorithms and their corresponding results. CB-CPW is selected over the conventional CPW configuration to avoid unwanted propagation modes at discontinuities such as the coupled slotline mode that degrades signal integrity and requires air-bridging [14].

CHAPTER 2. LITERATURE SURVEY

In the past, passive circuits based on microstrip line and CPW technology have been well developed. Microstrip structures are particularly suitable for the design of almost all passive microwave devices such as filters [15], hybrids and antennas [16-18]. CPW has the advantage of providing low dispersion and high isolation, [19] compared to microstrip line and can realize much more compact planar passives making it more attractive for modern wireless devices such as tables and smart phones. CPW filters can be realized by creating a discontinuity in the central strip [20], as slow-wave structures [21] or using loop resonators [22-23]. For the CPW-based filter applications such as bandpass filters (BPF) [24-28], band-reject filters (BRF) [29-31]. At the beginning of the design of BPFs, they are cascaded to achieve request of band-pass transmission characteristic [24], but this kind of filter structure is not compact, whose size is large compared with poor characteristics in band. A miniaturized double sided CPW BPF centered at 2.4 GHz is proposed in [25], where spurious response due to the center ground line is reduced by adding via in the electrode. The filter is much smaller than the conventional quarter wavelength CPW filter, but the suppression of harmonics is short in range. A compact sized BPF using slow-wave CPW tri-section stepped-Impedance resonators is also shown in [26] that provide easiness in the implementation to high-order filters. A CPW BPF with the hollow-T shaped transmission-line resonator is proposed in [27] for wide spurious suppression up to 11 GHz, but the size of the BPF is large compared to the above work stated. A compact CPW BPF [28] centered at 2.1 GHz where ultra-wide stopband is achieved up to 30 GHz using slow wave structure, but the circuit size is large as well. In [29], the band-reject characteristic of a slot-type split-ring resonator on a substrate used for microwave frequencies is presented which is very effective in rejecting unwanted frequency in terms of its selectivity and size. In [30], a broad-band BRF is developed using double-plane superposition, the obtained frequency response has big ripples in the higher pass-band. In [31], a photonic bandgap (PBG) structure constructed in CPW transmission line is used for broad-band BSF, but it occupies larger area because its PBG structure is implemented in the ground planes of the CPW transmission line.

The design of CPW-based LPFs with features like compact dimension, wide stopband with high stopband rejection, low insertion loss, and sharp roll-off is a task worth considering to microwave engineers. CPW technology provides convenient thin-film structure, requiring the

coating of only one side of the substrate and thereby simplifying the fabrication processing and assembly. Thus, the design of CPW-based LPFs has been widely addressed in recent research and a great amount of efforts has been made on that [32-40]. Various complicated patterns have been applied to the center conductor and ground plane of a transmission line in order to modulate its characteristic impedance [32]. Some interesting results have been obtained based on periodic perturbation of both signal line metallization and ground plane metallization on CPW LPF. In [33], a CPW LPF was designed based on cascading asymmetric LPF unit cells and dumbbell defected ground structures. The resulting design was compact with an extended stopband to seven times the cutoff frequency. However, the LPF costs too much because of the extra unit cells and the fabrication becomes difficult due to the employed cascaded structure. In [34], a CPW LPF was obtained by incorporating open stubs. The resulting design exhibited passband ripple in the range of 1.5 dB and a stopband rejection better than 45 dB. In [35], a design of wide stopband CPW LPF was achieved using three quarter wavelength stepped impedance resonators and a CPW spur line resonator. The fabricated LPF has deep attenuation from 3.7 GHz to 11 GHz lower than -24 dB. Nevertheless, the S parameters are not always good in pass band especially near to the cutoff frequency and the passband ripple is not reduced very well. In [36], stepped impedance resonators etched on the bottom of the substrate were used to design a CPW LPF. The measured stopband rejection was better than 30 dB up to 6.4 GHz, and a narrow transition band was obtained. However, substrate etching could cause more insertion losses. In [37], a bandwidth-tunable CPW LPF with broadband rejection was demonstrated by applying the varactor-tuned stub resonators. With them, the CPW LPF reaches a 65% bandwidth tuning range and a high broadband rejection greater than 15 dB at the frequencies up to 15 GHz. Yet, the resulting LPF is not compact and the structure is complicated regarding to the ease of fabrication. To reduce the size of a CPW LPF, a new application of micromachined overlay-coplanar-waveguide characterized by lifting the edges of the center conductors to facilitate low-impedance lines was developed in [38]. This method leads to a certain scale of length reduction around 20%; however, such technique considerably increases the complexity of the circuit. Another approach to miniaturize a CPW LPF is presented in [39]; a more compact CPW LPF in comparison to conventional ones was achieved by etching open complementary split ring resonators in the central strip. Nonetheless, this method adds much complexity to the circuit, as viaholes and underpaths are used. In order to suppress the spurious frequency bands, a new CPW LPF was described based on tapered periodic structures in [40].

Spurious frequency bands can be suppressed to below -22 dB at frequencies up to 20 GHz and passband ripples are negligible, and the return loss is better than 20 dB. However, this technique has poor impedance matching performance.

Besides, there have been increasing interests on microstrip/CB-CPW transition recently and a great amount of efforts have been made on that [41-48]. A 120 μm silicon substrate W band CB-CPW-to-microstrip transition which has 20% bandwidth and 0.2 dB insertion loss was proposed in [41]. [42] shows CB-CPW-to-microstrip transition to have a return loss less than -12 dB up to 14 GHz. In [43], a via free CB-CPW-microstrip transition at C-Band with return loss better than -15 dB from 2.8 to 7.5 GHz is developed. In [44], two CB-CPW-to-microstrip transitions with 1.4 dB insertion loss from 7 to 40 GHz are reported. In addition, in [45], a proposed CB-CPW-to-microstrip transition with via-holes drilled having a 3 dB back-to-back insertion loss bandwidth of 36 GHz is obtained. However, these transitions require very high dielectric constant substrates or suffer from narrow bandwidth. Also, some do not have good performance at lower frequencies.

CHAPTER 3. PROPOSED CB-CPW-BASED LPF DESIGNS

3.1 Structural Designs

Three types of CB-CPW structures are designed. For each design, the width of the signal trace of a conventional CB-CPW is varied to meet given LPF electrical characteristics (i.e., impedance matching, insertion loss) and physical constraints (i.e., minimum machinable width). The total length of the transmission line d is considered as one of the optimization variables for each structure as well. The filter termination impedance is 50Ω ; the highest practical line impedance is 136Ω , and the lowest is 14Ω . All designs are implemented on Rogers RO4003 substrate having 0.813-mm thickness H , with a relative permittivity ϵ_r of 3.55 and a dielectric loss tangent (i.e., $\tan \delta$) of 0.0027.

3.1.1 Type 1: CB-CPW with Varied Signal Trace and Constant Gap-to-trace Separation

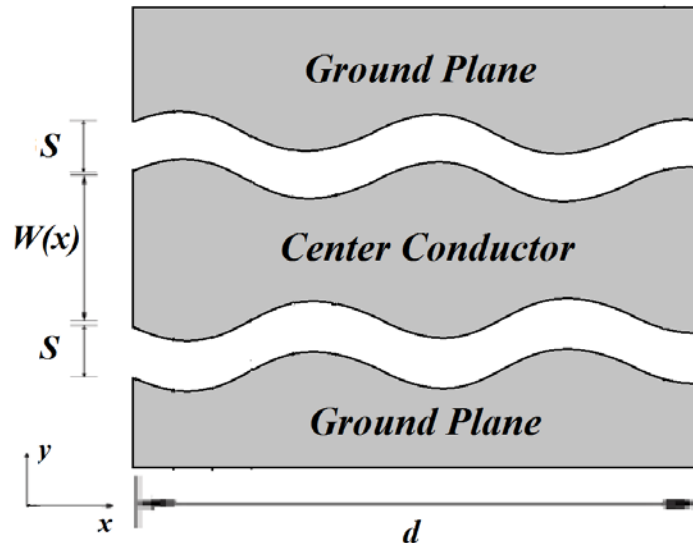


Figure 3 Top View of Type 1 Structure

A layout of the first designed CB-CPW model is shown in Figure 3. The ground-to-trace separation S is fixed to 2 mm, and the signal trace is varied as a function of horizontal position, expressed in $W(x)$. In this case, minimum and maximum values of $W(x)$ are set to 0.2 mm

(fabrication limit) and 10 mm. Furthermore, initial width of signal trace $W(0)$ and end point width $W(d)$ are both set to 1.9 mm due to 50Ω impedance matching.

3.1.2 Type 2: CB-CPW with Varied Signal Trace and Varied Gap-to-trace Separation

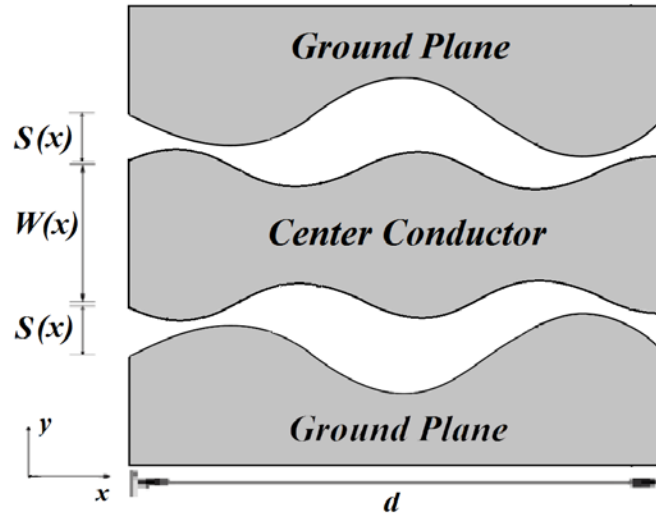


Figure 4 Top View of Type 2 Structure

As shown in Figure 4, compared to the first proposed structure, the width of gap S is no longer a constant. Instead, it is also modeled in a truncated Fourier series as $S(x)$. It is noteworthy to point out that in order to optimize this model under the same conditions, variations of $S(x)$ are set between 0.2 and 5.6 mm, and the variation of $W(x)$ is allowed between 0.24 and 9 mm. Similarly, $W(0)$ and $W(d)$ are 1.9 mm, $S(0)$ and $S(d)$ are set to 2 mm so that the impedance remains 50Ω at both ends.

3.1.3 Type 3: CB-CPW with Varied Signal Trace and Fixed Ground-to-ground Gap

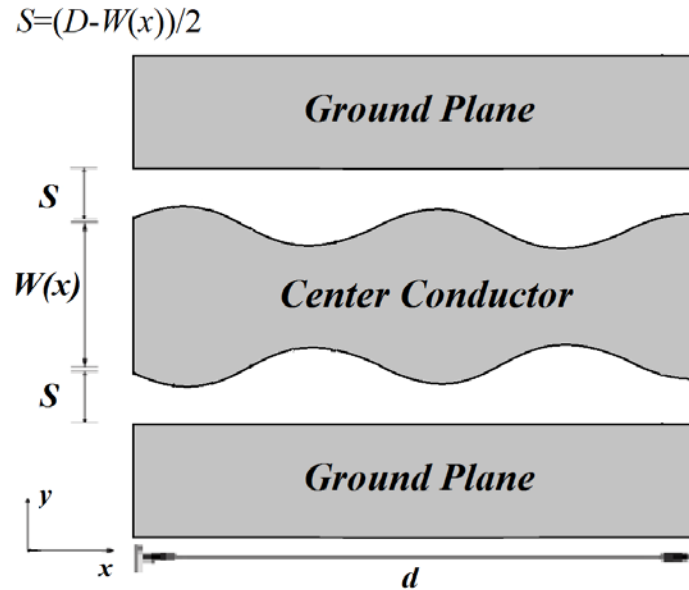


Figure 5 Top View of Type 3 Structure

As the name implies, Figure 5 shows that this case is defined as the sum of the width of gaps on both side and central signal trace is fixed to D . The signal trace is modeled in a truncated Fourier series, whereas the gap depends on $D = W(x) + 2S$. In type 1 and 2, the maximum values of D are 14 and 20.2 mm respectively. Thus, in order to get a similar LPF in size with same highest and lowest line impedances, $W(x)$ is set between 0.25 to 10.25 mm so that D ends up at 15.25 mm. Also, $W(0)$ and $W(d)$ are computed as 2.09 mm.

3.2 Mathematical Methodology

The non-uniform center conductor is subdivided into M short segments, each of a fixed length Δx . M is chosen such that $\Delta x \ll \lambda$, where λ is the guided wavelength at the cutoff frequency. The $ABCD$ parameters of the i^{th} segment ($i=1, 2, \dots, M$) at a frequency $f_j \in [0, f_{max}]$, where f_{max} is the highest frequency in the optimization interval, are given as [49]:

$$\begin{bmatrix} A & B \\ C & D \end{bmatrix}_i = \begin{bmatrix} \cos\theta_i & jZ_i \sin\theta_i \\ (j/Z_i) \sin\theta_i & \cos\theta_i \end{bmatrix}, \quad (1)$$

It is paramount to point out that lossless transmission lines are applied in this context. In (1), Z_i is the characteristic impedance at the center of each segment, given as [50]:

$$Z_i = \frac{60\pi}{\sqrt{\varepsilon_{eff}} \left[\frac{K(k_1) + K(k_2)}{K(k'_1) K(k'_2)} \right]}, \quad (2)$$

where $K(\cdot)$ is the complete non-linear elliptic integral of the first kind, $k'=(1-k^2)^{0.5}$, and ε_{eff} is the effective permittivity at the center of the i^{th} segment, which can be expressed as follows [50]:

$$\varepsilon_{eff} = \frac{1+\varepsilon_r \left[\frac{K(k'_1)/K(k_1)}{K(k_2)/K(k'_2)} \right]}{1+\left[\frac{K(k'_1)/K(k_1)}{K(k_2)/K(k'_2)} \right]}, \quad (3)$$

where ε_r is the relative substrate permittivity. ε_{eff} varies as a function of $W(x)$ as compared to conventional fixed-width CB-CPW configurations that possess a certain ε_{eff} . The ratios of the complete elliptic functions in (3) can be approximated as given in [51]:

$$\frac{K(k)}{K(k')} \cong \begin{cases} \frac{1}{2\pi} \ln \left[2 \frac{\sqrt{1+k} + \sqrt[4]{4k}}{\sqrt{1+k} - \sqrt[4]{4k}} \right] & 1 \leq \frac{K(k)}{K(k')} \leq \infty, \frac{1}{\sqrt{2}} \leq k \leq 1 \\ \frac{2\pi}{\ln \left[2 \frac{\sqrt{1+k'} + \sqrt[4]{4k'}}{\sqrt{1+k'} - \sqrt[4]{4k'}} \right]} & 0 \leq \frac{K(k)}{K(k')} \leq 1, 0 \leq k \leq \frac{1}{\sqrt{2}} \end{cases} \quad (4)$$

In (2) and (3), the parameters k_1 and k_2 are width-dependent, and can be calculated as [50]:

$$k_1 = \frac{W(x)}{W(x) + 2S(x)}, \quad (5.a)$$

$$k_2 = \frac{\tanh[\pi W(x)/4h]}{\tanh\{\pi[W(x) + 2S(x)]/4h\}}, \quad (5.b)$$

In (5), $S(x)$ represents the gap between the signal trace and adjacent ground planes, and H is the substrate thickness. The electrical length at the center of the i^{th} segment, θ_i , is expressed as [49]:

$$\theta_i = \frac{2\pi}{\lambda} \Delta x = \frac{2\pi}{c} f_j \sqrt{\varepsilon_{eff}} \Delta x, \quad (6)$$

where c is the speed of light. The non-uniform width, $W(x)$ or non-uniform gap $S(x)$ in second proposed design are expressed in terms of a truncated Fourier series expansion as follows [52]:

$$W(x) = W_{ref} \exp \left\{ c_0 + \sum_{n=0}^N \left[a_n \cos\left(\frac{2\pi n x}{d}\right) + b_n \sin\left(\frac{2\pi n x}{d}\right) \right] \right\}, \quad (7)$$

where W_{ref} is a reference width. The N series coefficients, c_0 , a_n , and b_n are set as optimization variables. $2N + 1$ Fourier coefficients are bounded within the interval $[-2,2]$ to reduce the search space, and the length d is bounded within the interval $[40,100]$. The $ABCD$ matrix of entire structure can be obtained by multiplying the $ABCD$ matrices of all M segments as follows [52]:

$$[A \ B; C \ D] = \prod_{i=1}^M [A \ B; C \ D]_i \quad (8)$$

Then, the scattering parameters can be expressed in terms of the overall $ABCD$ matrix. The input port matching, S_{11} , and transmission parameter, S_{21} , of the CB-CPW LPF are provided as follows [52]:

$$S_{11} = \frac{A + B/Z_0 - CZ_0 - D}{A + B/Z_0 + CZ_0 + D}, \quad (9.a)$$

$$S_{21} = \frac{2(AD - BC)}{A + B/Z_0 + CZ_0 + D}, \quad (9.b)$$

where Z_0 is the characteristic impedance of the input/output ports (set to $50 \ \Omega$ to match the impedance of the end-termination connectors). In order for the CPW line to function as a LPF, the following error function is considered at each frequency f_j with step size Δf , in a frequency range $[0, f_{max}]$:

$$Error = \begin{cases} 100|S_{11}|^2 & 0 \leq f_j \leq f_p \\ (|S_{21}| - 10^{-\frac{\alpha_r [dB]}{20}})^2 & f_p < f_j \leq f_s \\ 50(|S_{21}| - \alpha_s)^2 & f_s < f \leq f_{max}, |S_{21}| > \alpha_s \\ 0 & f_s < f \leq f_{max}, |S_{21}| \leq \alpha_s \end{cases} \quad (10)$$

where f_p is the cutoff frequency of the designed LPF, α_s is the transmission loss in the stopband range $(f_s, f_{max}]$, and $\alpha_r = \alpha_p + (\alpha_s - \alpha_p)(f_j - f_p)/(f_s - f_p)$ is a frequency-dependent parameter that controls the transmission loss roll-off in the range $(f_p, f_s]$ where α_p is the desired transmission loss in the passband range $(0, f_p]$ [53]. The error vector resulting from applying (10) to all frequency point within $[0, f_{max}]$ is used to establish the following *Objective* function as follows:

$$Objective = \sqrt{\frac{1}{N_f} \sum_{p=0}^{N_f} Error}, \quad (11)$$

where $N_f = f_{max}/\Delta f$ is the number of frequency point. Finally the summation of the errors at all frequencies is minimized subject considering the following constraints that ensure physical matching and realization of practical widths:

$$W_{min} \leq W(x) \leq W_{max}, \quad (12.a)$$

$$W(0) = W(d) = W_{ref}, \quad (12.b)$$

The constraint presented in (12.a) confines the width profile within fabrication limitations. And (12.b) ensures that both CB-CPW LPF terminations are equal and match up with the 50 Ω standard connector. It is achieved by satisfying following condition:

$$c_0 + \sum_{n=1}^N a_n = 0 \quad (13)$$

3.3 Analytical Results

In this section, a design example of a non-uniform CB-CPW LPF is presented. The cutoff frequency is set to $f_p = 2$ GHz, stopband start with $f_s = 3$ GHz, $f_{max} = 6$ GHz, and the frequency step size $\Delta f = 0.2$ GHz. Transmission loss in the passband is set to $\alpha_p = 0$ dB; while in the stopband, $\alpha_s = -30$ dB. The M uniform segments and the N Fourier terms in $W(x)$ are set to 50 and 5 respectively, which are sufficient to achieve the required goals. The minimization of the *Objective* function in (11) is carried out using three specific optimization techniques. Specifically, (1) Trust-region-reflective algorithm (TRRA): a local optimizer known for its robustness in solving constrained nonlinear minimization problems [54]; (2) Genetic algorithm (GA): a widely used global optimization that has been applied in microwave-related problems [55-56]; (3) Particle swarm optimization algorithm (PSO): a global optimization algorithms having a few adjustable parameters that is simple in construction and can be easily applied to diverse issues [57]. The optimization techniques are performed in 1000 iterations or generations using MATLAB. Furthermore, the tolerance interval on the *Objective* function, physical constraints, and Fourier coefficients between two iterations is set to 10^{-20} .

3.3.1 Type 1

A. Trust-region-reflective Algorithm

As shown in Figure 6, the optimized width profile of the signal trace of type 1 CB-CPW LPF has been generated from TRRA. The maximum and minimum widths are 7.8 mm and 0.251 mm, and $W(0) = W(d) = W_{ref} = 1.9$ mm. Thus, it demonstrates that the profile is constrained by the predefined physical constraints and follows (12.a) and (12.b). The width of gap is fixed to 2 mm throughout the first type designs. In addition, the optimized CB-CPW is 71.6385 mm long as the result of length optimization.

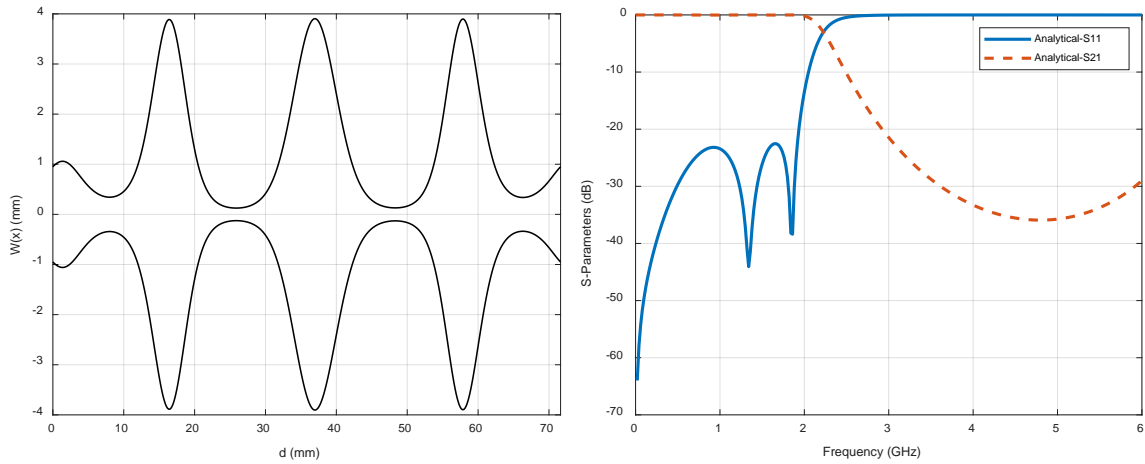


Figure 6 Type 1 Optimized Width Profile Using TRRA with Corresponding Analytical Response

Figure 6 also shows the analytical result of the optimized type 1 CB-CPW LPF over a frequency range $[0, f_{max}]$ when TRRA is adopted. S_{11} is better than -20 dB within $[0, f_p]$ passband and an attenuation better than -30 dB is obtained in $(f_s, f_{max}]$ stopband. Besides, S_{21} reaches -20 dB at $f_s = 3$ GHz. Hence, the first proposed type of CB-CPW LPF satisfied with predefined conditions is gathered.

B. Genetic Algorithm

As shown in Figure 7, the optimized width profile of the signal trace of type 1 CB-CPW LPF has been generated from GA. The maximum and minimum widths are 9.1 mm and 0.213 mm, and $W(0) = W(d) = W_{ref} = 1.9$ mm. Thus, it demonstrates that the profile is constrained by the

predefined physical constraints and meets the conditions (12.a) and (12.b) as well. In addition, the optimized CB-CPW is 77.7771 mm long as the result of length optimization.

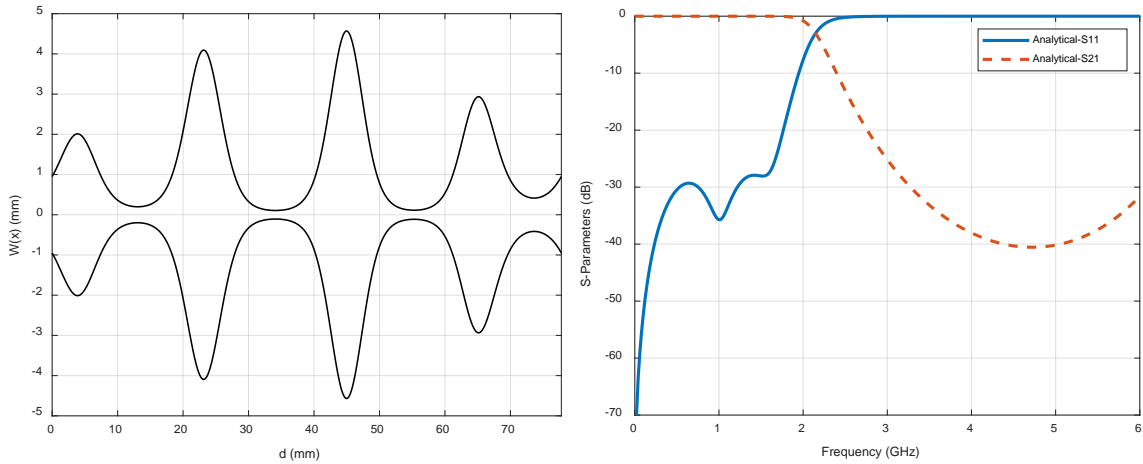


Figure 7 Type 1 Optimized Width Profile Using GA with Corresponding Analytical Response

Figure 7 also shows the analytical result of the optimized type 1 CB-CPW LPF over a frequency range $[0, f_{max}]$ when GA is adopted. S_{11} is roughly better than -30 dB within $[0, 1]$ GHz; however it rises to around -10dB at the cutoff frequency $f_p = 2$ GHz. And an attenuation ends up to -40 dB is obtained at around 5 GHz. Besides, S_{21} reaches -25dB at f_s . Hence, the first proposed type of CB-CPW LPF satisfied with predefined conditions is gathered.

C. Particle Swarm Optimization Algorithm

As shown in Figure 8, the optimized width profile of the signal trace of type 1 CB-CPW LPF has been generated from PSO. The maximum and minimum widths are 10 mm and 0.194 mm, and $W(0) = W(d) = W_{ref} = 1.9$ mm. Thus, it implies that the optimized profile follows (12.b); whereas it doesn't reach (12.a) and has 0.006 mm error which is acceptable. In addition, the optimized CB-CPW is 52.4717 mm long as the result of length optimization which is the most miniaturized result of the first type compared to TRRA and GA.

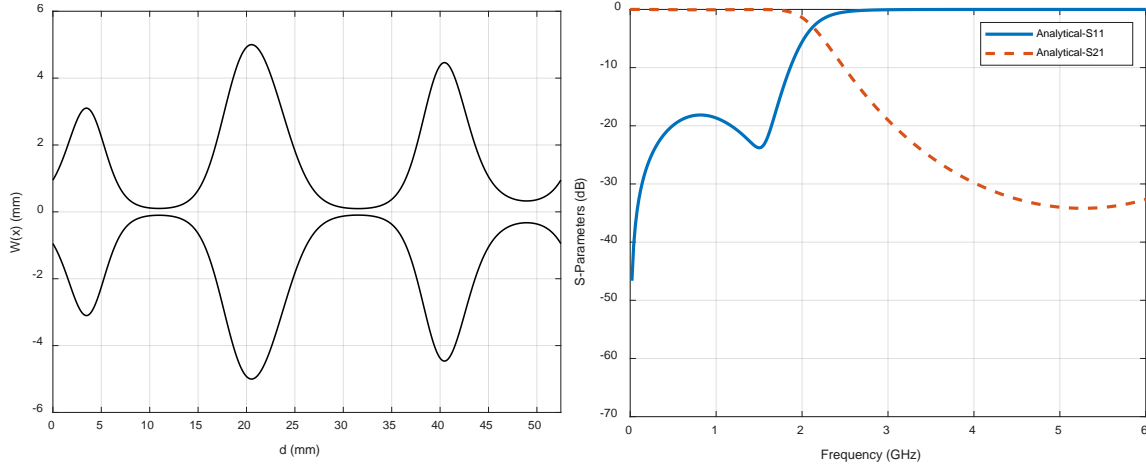


Figure 8 Type 1 Optimized Width Profile Using PSO with Corresponding Analytical Response

Figure 8 also shows the analytical result of the optimized type 1 CB-CPW LPF over a frequency range $[0, f_{max}]$ when PSO is adopted. S_{11} is better than -15 dB within $[0, f_p]$ passband and an attenuation better than -30 dB is obtained in $(f_s, f_{max}]$ stopband. Besides, S_{21} almost reaches -20 dB at $f_s = 3$ GHz. Hence, the first proposed type of CB-CPW LPF satisfied with predefined conditions is gathered.

3.3.2 Type 2

A. Trust-region-reflective Algorithm

Unlike the first type design, the structures for both signal trace and gaps are modeled and optimized. As shown in Figure 9, the optimized width profile of type 2 CB-CPW LPF has been generated from TRRA. The maximum and minimum widths for signal trace W are 6.8 mm and 0.339 mm, and $W(0) = W(d) = W_{ref} = 1.9$ mm. Moreover, the maximum and minimum widths for gaps S are 2.3 mm and 2 mm, and $S(0) = S(d) = S_{ref} = 2$ mm. Not only signal traces plotted in solid lines but also gaps in broken lines demonstrate that the profile is constrained by the predefined physical constraints and follows (12.a) and (12.b). It is worthy to point out that the gaps are found out to be 2 ± 0.3 mm although the variation is allowed between 0.2 mm to 5.6 mm as mentioned before. In addition, the optimized CB-CPW is 76.8268 mm long as the result of length optimization.

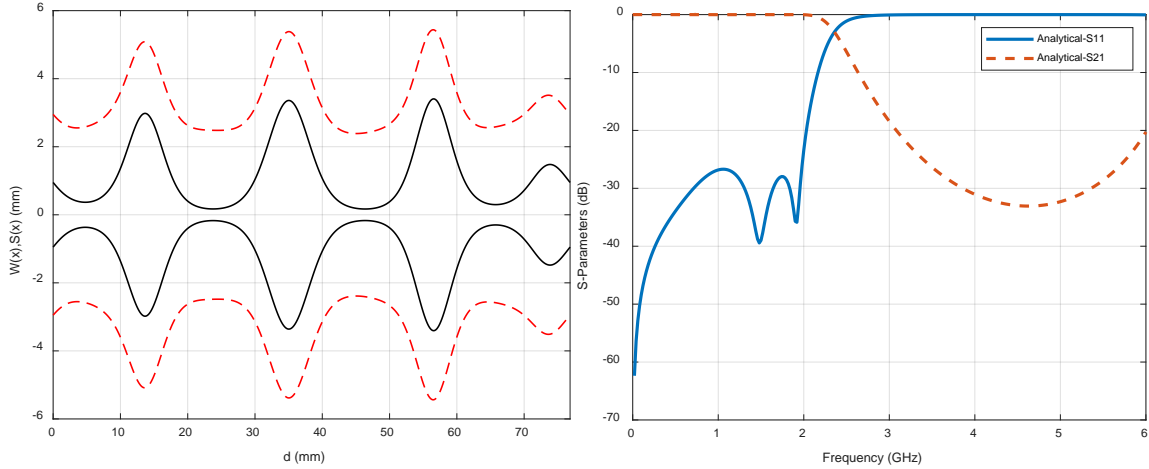


Figure 9 Type 2 Optimized Width Profile Using TRRA with Corresponding Analytical Response

Figure 9 also shows the analytical result of the optimized type 2 CB-CPW LPF over a frequency range $[0, f_{max}]$ when TRRA is adopted. S_{11} is better than -25 dB within $[0, f_p]$ passband and an attenuation better than -30 dB is obtained in (f_s, f_{max}) stopband. Besides, S_{11} is better than -20 dB at the cutoff frequency $f_p=2$ GHz and S_{21} almost reaches -20 dB at $f_s=3$ GHz. Hence, the second proposed type of CB-CPW LPF satisfied with predefined conditions is gathered.

B. Genetic Algorithm

As shown in Figure 10, the optimized width profile of type 2 CB-CPW LPF has been generated from GA. The maximum and minimum widths for signal trace W are 9 mm and 0.234 mm, and $W(0) = W(d) = W_{ref} = 1.9$ mm. Moreover, the maximum and minimum widths for gap S are 5.7 mm and 0.192 mm, and $S(0) = S(d) = S_{ref} = 2$ mm. In this case, the gap takes up all the variation which is set between 0.2 mm to 5.6 mm even more. In addition, the optimized CB-CPW is 53.4565 mm long as the result of length optimization. It is the most compact proposed second type of CB-CPW LPF design. Nevertheless, its EM performance is unsatisfactory compared to others.

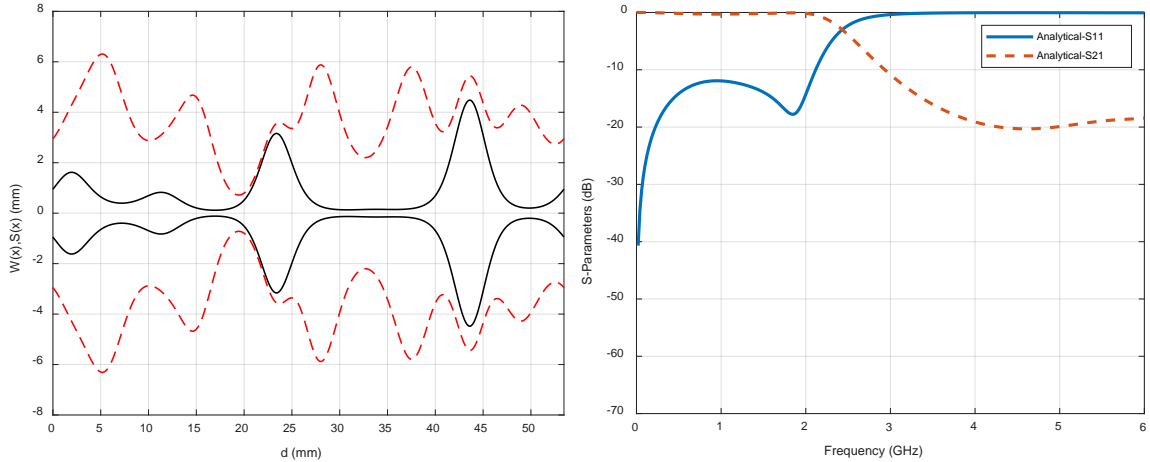


Figure 10 Type 2 Optimized Width Profile Using GA with Corresponding Analytical Response

Figure 10 also shows the analytical result of the optimized type 2 CB-CPW LPF over a frequency range $[0, f_{max}]$ when GA is adopted. S_{11} is better than -10 dB within $[0, f_p]$ passband. And an attenuation of -20 dB is obtained in $(f_s, f_{max}]$ stopband. Hence, due to the plenty of time GA taking, the second proposed type of CB-CPW LPF ends up with this optimal design.

C. Particle Swarm Optimization Algorithm

As shown in Figure 11, the optimized width profile of type 2 CB-CPW LPF has been generated from PSO. The maximum and minimum widths for signal trace W are 9.1 mm and 0.237 mm, and $W(0) = W(d) = W_{ref} = 1.9$ mm. Moreover, the maximum and minimum widths for gaps S are 5.6 mm and 0.199 mm, and $S(0) = S(d) = S_{ref} = 2$ mm. It implies that the optimized profile follows (12.b), and has negligible error regarding to (12.a). Similar to GA, the gap takes up all the variation which is between 0.2 mm to 5.6 mm and even more. In addition, the optimized CB-CPW is 56.8612 mm long as the result of length optimization which is fairly good in size.

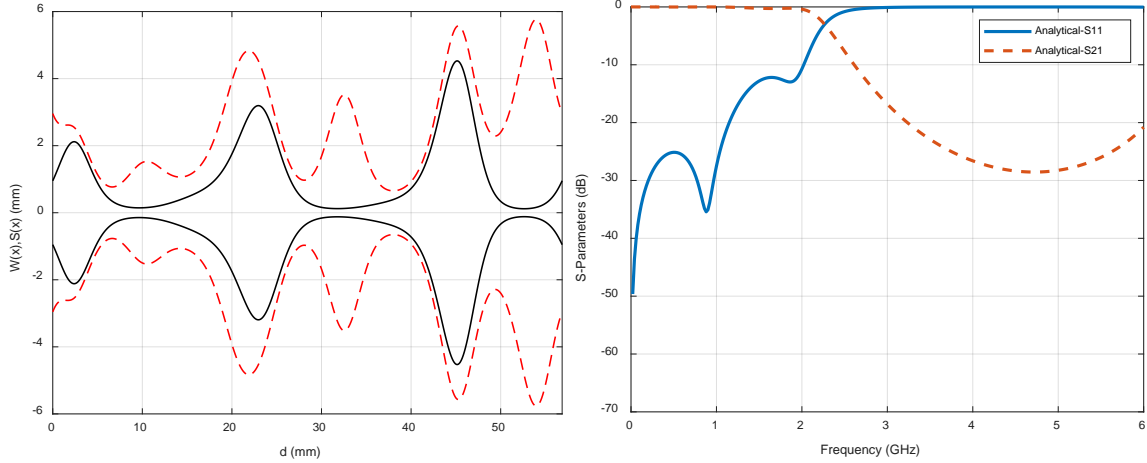


Figure 11 Type 2 Optimized Width Profile Using PSO with Corresponding Analytical Response

Figure 11 also shows the analytical result of the optimized type 2 CB-CPW LPF over a frequency range $[0, f_{max}]$ when PSO is adopted. S_{11} is better than -25 dB within $[0, 1]$ GHz; however, it gets -10 dB at the cutoff frequency $f_p = 2$ GHz. An attenuation better than -25 dB is obtained in $(f_s, f_{max}]$ stopband. Besides, S_{21} almost reaches -15 dB at $f_s = 3$ GHz. Hence, the second proposed type of CB-CPW LPF satisfied with predefined conditions is gathered.

3.3.3 Type 3

A. Trust-region-reflective Algorithm

As shown in Figure 12, the optimized width profile of signal trace of type 3 CB-CPW LPF has been generated from TRRA. The maximum and minimum widths are 8.4 mm and 0.407 mm, and $W(0) = W(d) = W_{ref} = 2.09$ mm. It demonstrates that the profile is constrained by the predefined physical constraints and follows (12.a) and (12.b). The width of gap is calculated by $S = (D - W(x)) / 2$ throughout the third type designs, where D is fixed to 15.25 mm. In addition, the optimized CB-CPW is 71.0510 mm long as the result of length optimization.

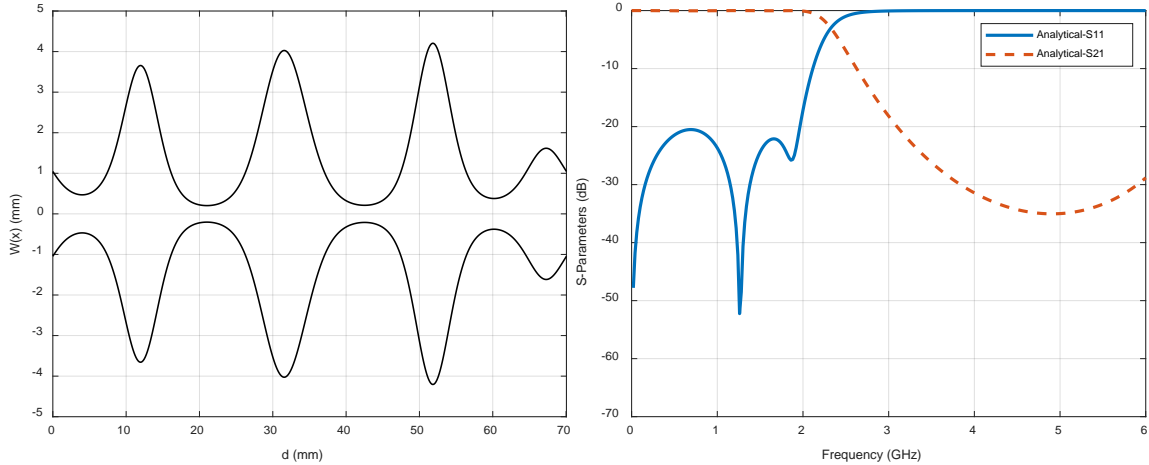


Figure 12 Type 3 Optimized Width Profile Using TRRA with Corresponding Analytical Response

Figure 12 also shows the analytical result of the optimized type 3 CB-CPW LPF over a frequency range $[0, f_{max}]$ when TRRA is adopted. S_{11} is better than -20 dB within $[0, f_p]$ passband and an attenuation better than -30 dB is obtained in $(f_s, f_{max}]$ stopband. Besides, S_{21} almost reaches -20 dB at $f_s=3$ GHz. Hence, the third proposed type of CB-CPW LPF satisfied with predefined conditions is gathered.

B. Genetic Algorithm

As shown in Figure 13, the optimized width profile of signal trace of type 3 CB-CPW LPF has been generated from GA. The maximum and minimum widths are 9.2 mm and 0.273 mm, and $W(0) = W(d) = W_{ref} = 2.09$ mm. It demonstrates that the profile is constrained by the predefined physical constraints and follows (12.a) and (12.b). In addition, the optimized CB-CPW is 56.4111 mm long as the result of length optimization. This design performs well on both complexity and EM characteristics.

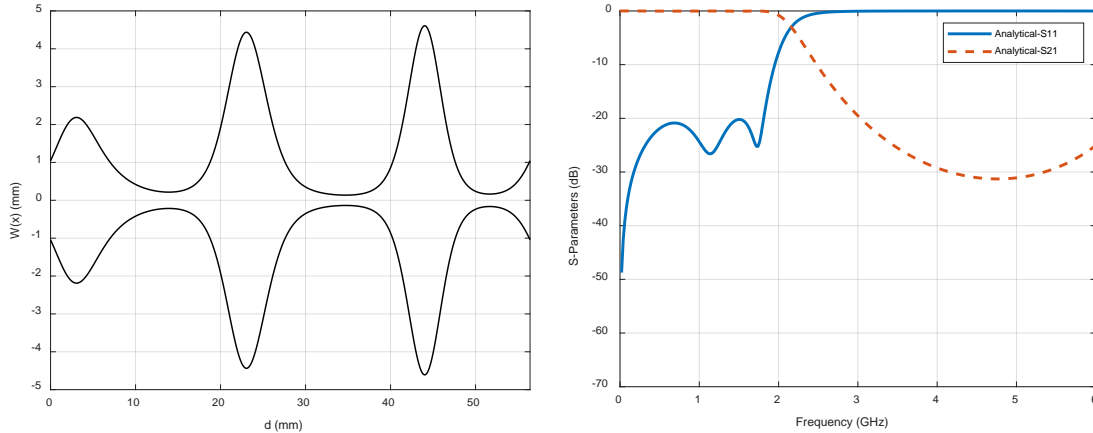


Figure 13 Type 3 Optimized Width Profile Using GA with Corresponding Analytical Response

Figure 13 also shows the analytical result of the optimized type 3 CB-CPW LPF over a frequency range $[0, f_{max}]$ when GA is adopted. S_{11} is better than -20 dB within $[0, f_p]$ passband and an attenuation better than -30 dB is obtained in $(f_s, f_{max}]$ stopband. Besides, S_{21} almost reaches -20 dB at $f_s = 3$ GHz. Hence, the third proposed type of CB-CPW LPF satisfied with predefined conditions is gathered.

C. Particle Swarm Optimization Algorithm

As shown in Figure 14, the optimized width profile of the signal trace of type 3 CB-CPW LPF has been generated from PSO. The maximum and minimum widths are 10.7 mm and 0.242 mm, and $W(0) = W(d) = W_{ref} = 2.09$ mm. It implies that the profile follows (12.b). Nonetheless, the signal trace slightly exceeds the variation which is set between 0.25 mm and 10.05 mm. In addition, the optimized CB-CPW is 83.3825 mm long as the result of length optimization which lacks of improvement regarding to size.

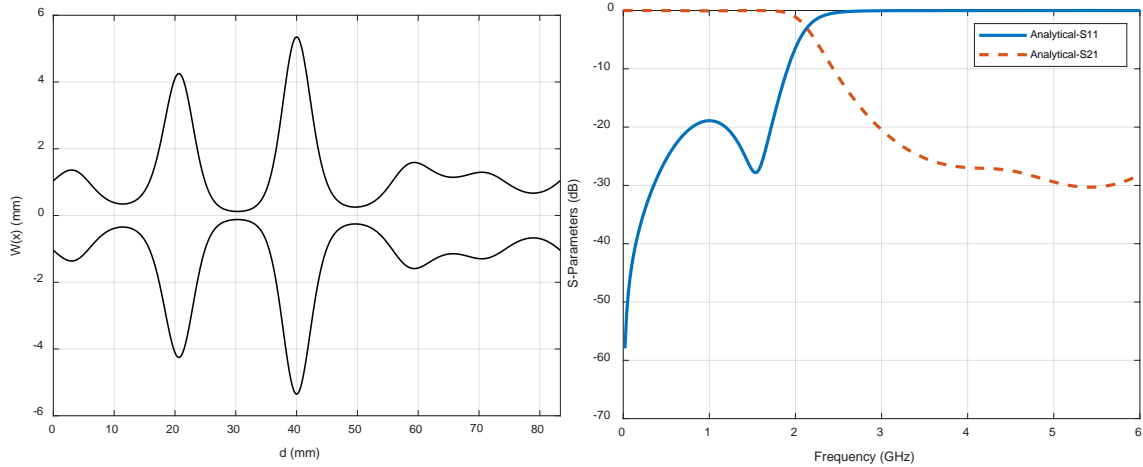


Figure 14 Type 3 Optimized Width Profile Using PSO with Corresponding Analytical Response

Figure 14 also shows the analytical result of the optimized type 3 CB-CPW LPF over a frequency range $[0, f_{max}]$ when PSO is adopted. S_{11} is roughly better than -20 dB within $[0, f_p]$ passband and an attenuation equals to -30 dB is obtained at around 5.4 GHz. Besides, S_{21} reaches -20 dB at $f_s=3$ GHz; whereas S_{11} goes up to undesired -5 dB. Hence, the third proposed type of CB-CPW LPF is gathered.

Furthermore, corresponding resulting optimized Fourier series coefficients of each algorithm are recorded and provided in Table 1, Table 2 and Table 3.

Table 1 Type 1 Optimized Fourier Series Coefficients

	c_0	a_1	a_2	a_3	a_4	a_5
TRRA	-0.1967	0.0129	0.0013	0.0265	0.0010	-1.0187
GA	-0.2370	0.1388	0.0165	0.0356	-0.0595	0.1436
PSO	-0.1177	0.0141	-0.0503	0.0480	-0.8533	0.1537
	b_1	b_2	b_3	b_4	b_5	
TRRA	-0.3467	0.8394	0.4029	0.3366	0.2367	
GA	-0.7724	-0.1474	1.3229	0.0663	0.1842	
PSO	1.4728	0.0832	0.3712	-0.1812	0.0131	

Table 2 Type 2 Optimized Fourier Series Coefficients

	c_0	a_1	a_2	a_3	a_4	a_5
TRRA	-0.1739	0.0268	-0.0085	0.0061	0.0238	-0.4492
GA	-0.0924	-0.0673	0.1068	0.0753	-0.3284	0.1722
PSO	-0.4542	-0.0198	-0.0933	-0.2752	-0.7084	0.2446
	b_1	b_2	b_3	b_4	b_5	
TRRA	0.5764	0.5138	-0.8938	0.0764	-0.2758	
GA	1.0103	-0.3490	0.6302	0.2612	0.3824	
PSO	1.1672	0.1810	0.4290	0.3260	0.3592	
	c_1	a_6	a_7	a_8	a_9	a_{10}
TRRA	0.0729	0.0048	0.0075	-0.0168	0.0079	0.0112
GA	-0.4082	0.2766	0.2812	0.0652	0.9148	-0.8480
PSO	-0.6900	0.1253	-0.0186	0.3551	-0.5060	-0.0306
	b_6	b_7	b_8	b_9	b_{10}	
TRRA	-0.0224	-0.0431	0.0197	-0.0291	0.0157	
GA	0.2382	0.6967	0.5277	0.2178	-0.0437	
PSO	-0.7254	-0.2059	0.0368	0.4481	-0.5397	

Table 3 Type 3 Optimized Fourier Series Coefficients

	c_0	a_1	a_2	a_3	a_4	a_5
TRRA	-0.0674	0.0058	-0.0065	0.0282	-0.0073	-0.4759
GA	-0.3678	0.0278	0.0786	0.0355	-0.5006	-0.1328
PSO	-0.1320	0.0403	-0.0880	-0.0630	-0.0431	-0.4153
	b_1	b_2	b_3	b_4	b_5	
TRRA	0.6787	0.4121	-0.8281	0.0972	-0.3470	
GA	1.3994	0.1678	0.2442	0.2695	-0.0209	
PSO	-0.0508	0.8873	-0.2093	-0.3174	0.6194	

3.3.4 Comparison between Three Algorithms

A comparison between the three adopted algorithms is shown in following tables. In conclusion, TRRA generally requires minimum optimization time at the expense of higher error because it works as a local optimizer that depends on the derivative of the *Objective* function instead of globally searching the space like GA. Also, it can be seen from the results that TRRA strictly follow the predefined constraints as its robustness. On the other hand, GA executes much more time for solutions due to its high exploration ability. As for PSO, it falls in between TRRA and GA. It has moderate accuracy within a small amount of time compared to GA because of its premature convergence. However, it has a tendency to get stuck in a near optimal solution

especially for middle and large size problems and it is difficult to improve solution accuracy by fine-tuning parameters.

Table 4 Comparison between the Three Algorithms on Type 1

	Population Size	Avg. Execution Time per Single Run(sec)	Value of the Objective
TRRA	/	2257	0.4945
GA	50	8215	0.3679
PSO	50	5318	0.4376

Table 5 Comparison between the Three Algorithms on Type 2

	Population Size	Avg. Execution Time per Single Run(sec)	Value of the Objective
TRRA	/	7711	0.2842
GA	50	24681	0.4817
PSO	50	14048	0.3841

Table 6 Comparison between the Three Algorithms on Type 3

	Population Size	Avg. Execution Time per Single Run(sec)	Value of the Objective
TRRA	/	2975	0.4120
GA	50	9101	0.3118
PSO	50	6192	0.3569

Also, the analytical results for three algorithms considering type 1 CB-CPW as representative are displayed in one picture. The results of input port matching S_{11} and transmission parameter S_{21} are presented in Figure 15.

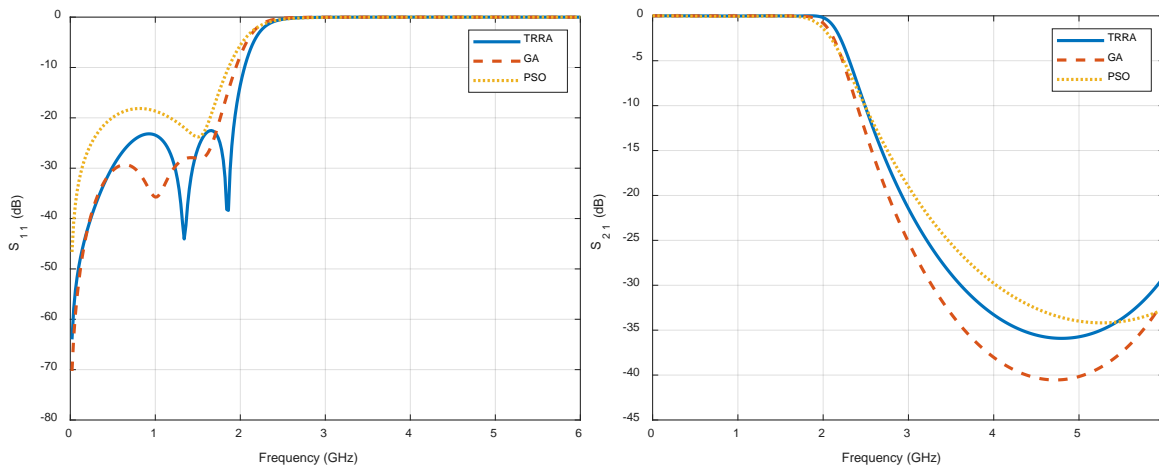


Figure 15 Type 1 Comparison of Analytical Results between Three Algorithms

Consequently, in the first type of design, PSO has the worst performance in the aspect of input port matching. It is because the trade-off between compactness and EM performance is taken into account as the most compact design with length d of 52.4717 mm is obtained from PSO compared to 71.6385 mm from TRRA and 77.7771 mm from GA. The trade-off takes place between compactness and EM performance. And GA obtains the best transmission parameter due to long simulation time.

3.3.5 Comparison between Three Proposed Types of Structures

In order to decide which type of design has the best performance considering fabrication difficulties, flexibility and EM characteristics, the analytical results of different applied structures are plotted in one considering TRRA as representative. It is also worth noting that the optimized length d of three types of designs are rather close as 71.6385 mm, 76.8268 mm and 71.0510 mm respectively.

As shown in Figure 16, the type 2 design with varied gap S has noticeable better performance among three designs regarding to input port matching as S becomes another variable being optimized and more flexibilities are added to this type of design. Figure 16 also clarifies that all types of designs satisfy with predefined -30 dB transmission loss in the stopband range (3,6] GHz, and type 1 design with constant gap performs approximately 2.5 dB better than other types.

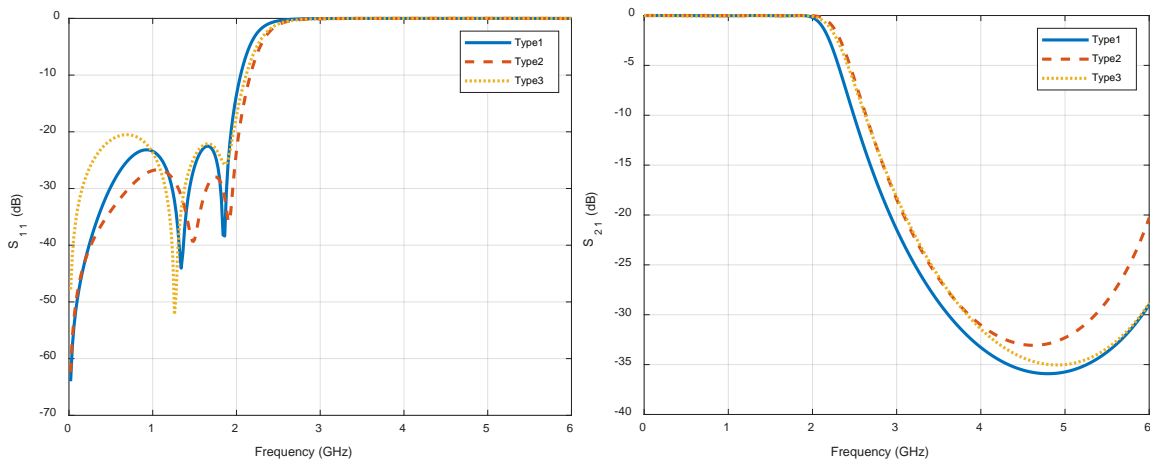


Figure 16 Comparison of Analytical Results Using TRRA between Three Types of Designs

3.4 Simulated Results

In this section, all the width profiles are exporting to AutoCAD to get DXF files which can be read by EM simulation solver Ansys High Frequency Structure Simulation (HFSS) [58]. Once the 2-dimensional profile is drawn in AutoCAD, we can import it to HFSS and start building the 3D model according to following general steps.

Step-1: Expand the Z dimension according to the thickness of the substrate, and assign material to the substrate.

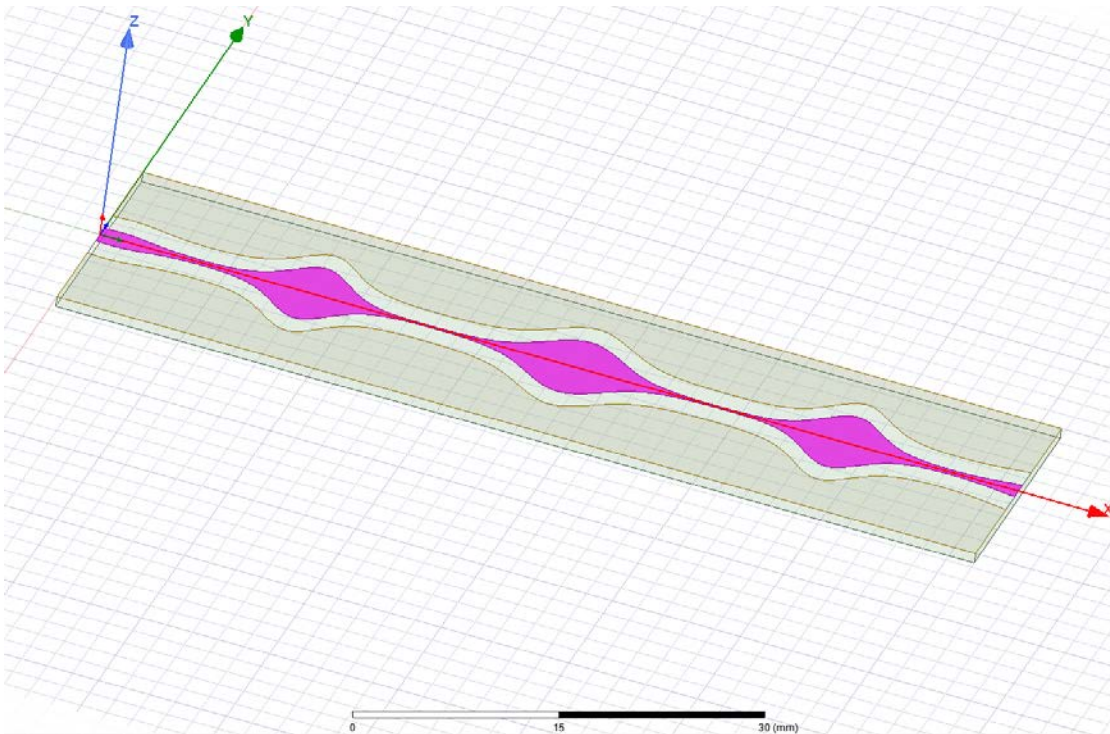


Figure 17 Schematic of the 3D model

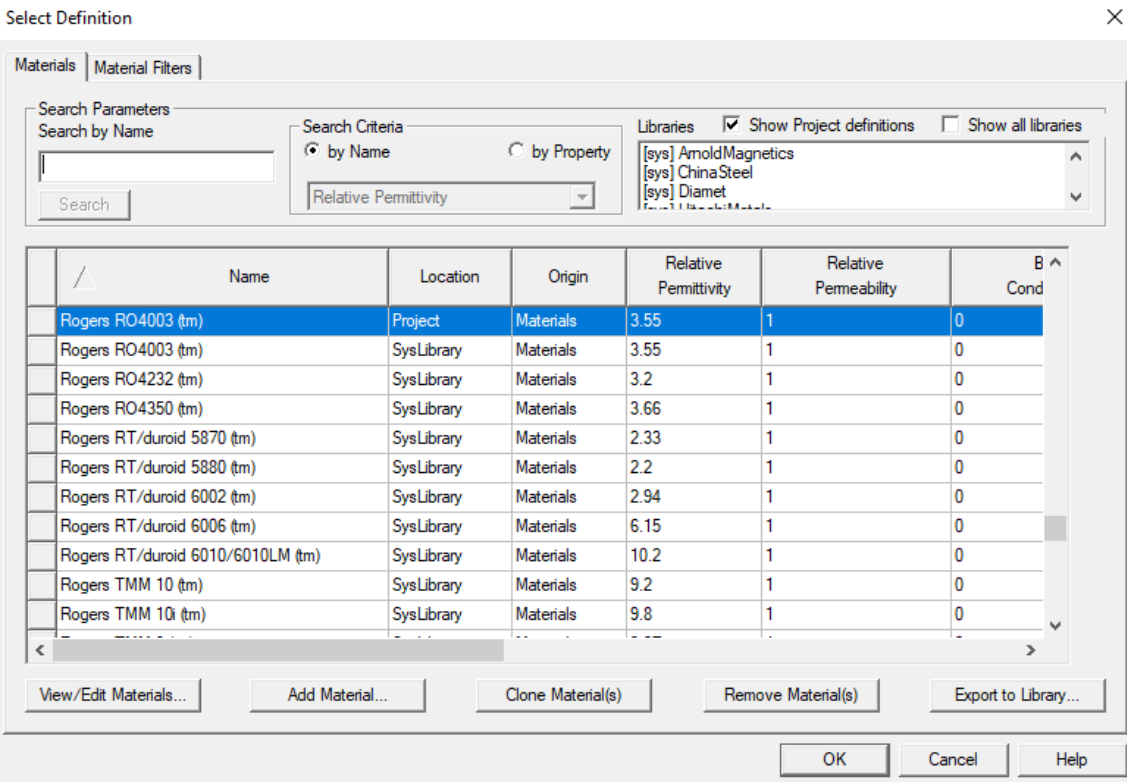


Figure 18 Interface of Assigning Material

Step-2: Assign boundary to each unassigned object including ground.

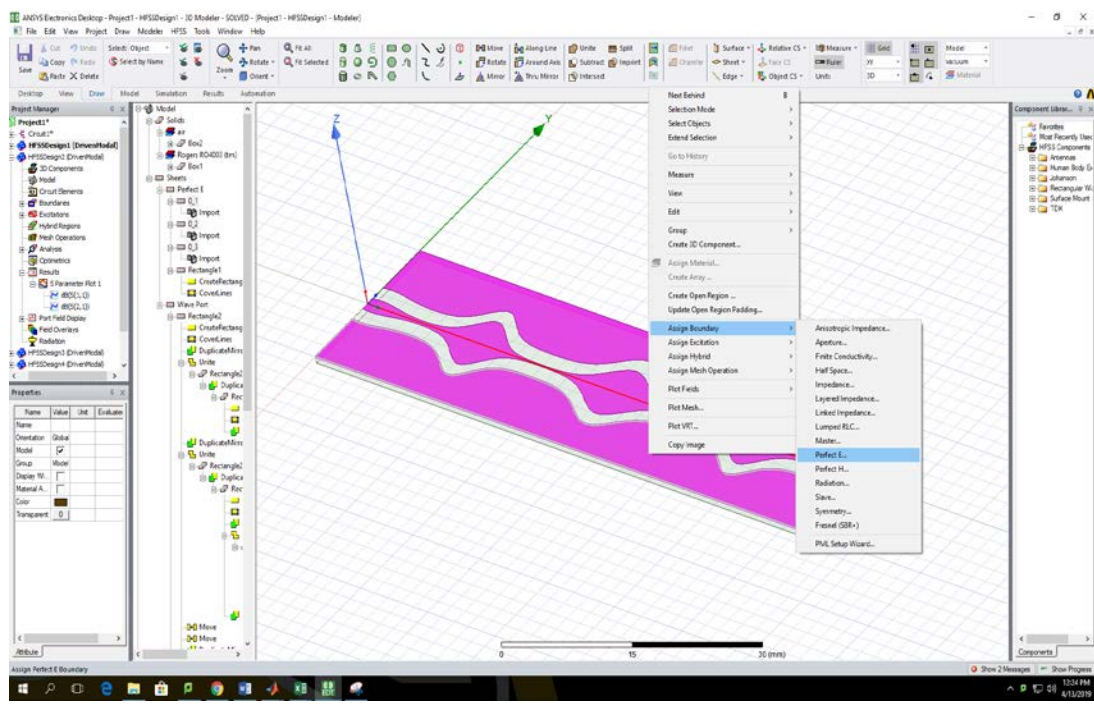


Figure 19 Interface of Assigning Boundary

Step-3: Create air-filled box and assign its boundary as radiation.

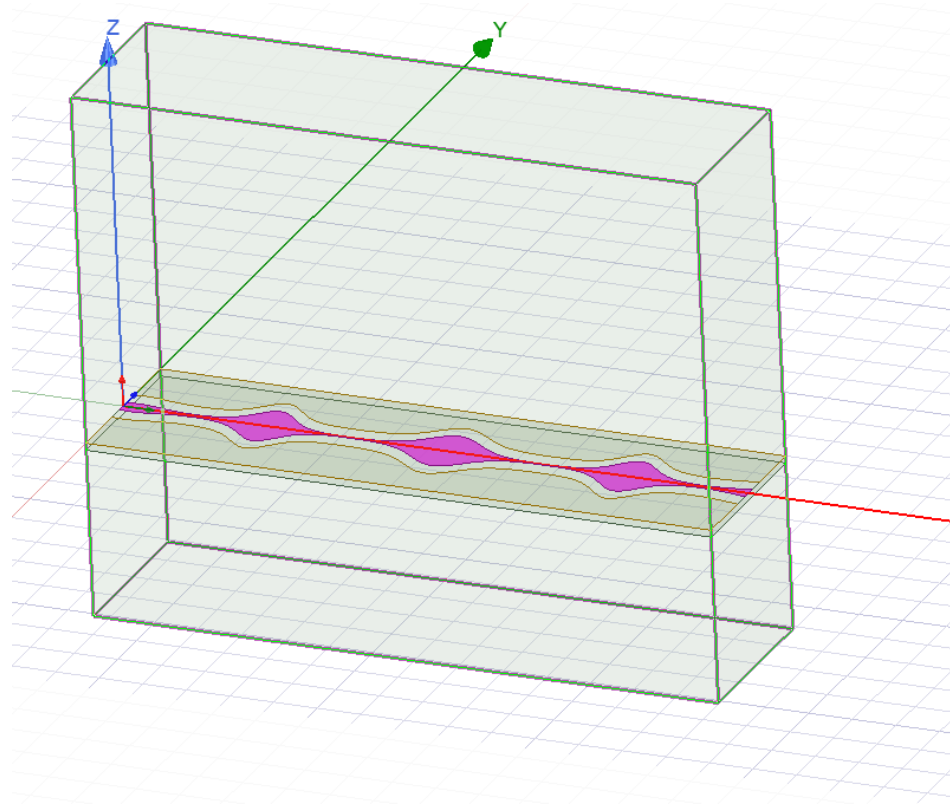


Figure 20 Schematic of the Radiation Box

Step-4: Assign excitations at both ends.

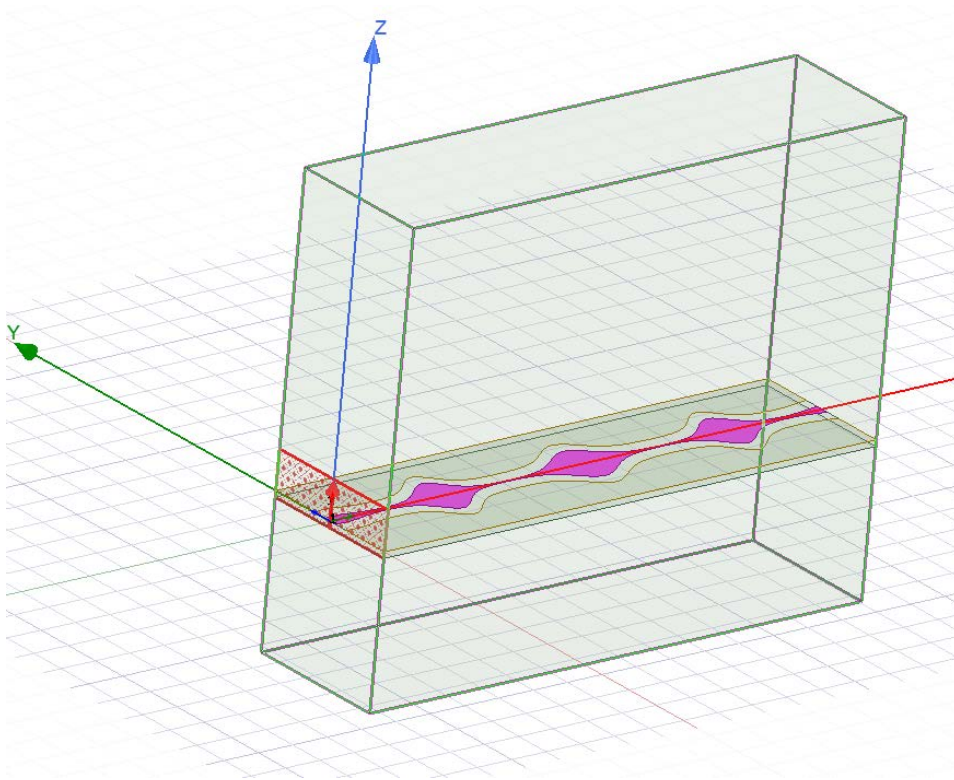


Figure 21 Schematic of the Excitation Surface

Step-5: Set up the simulation configurations.

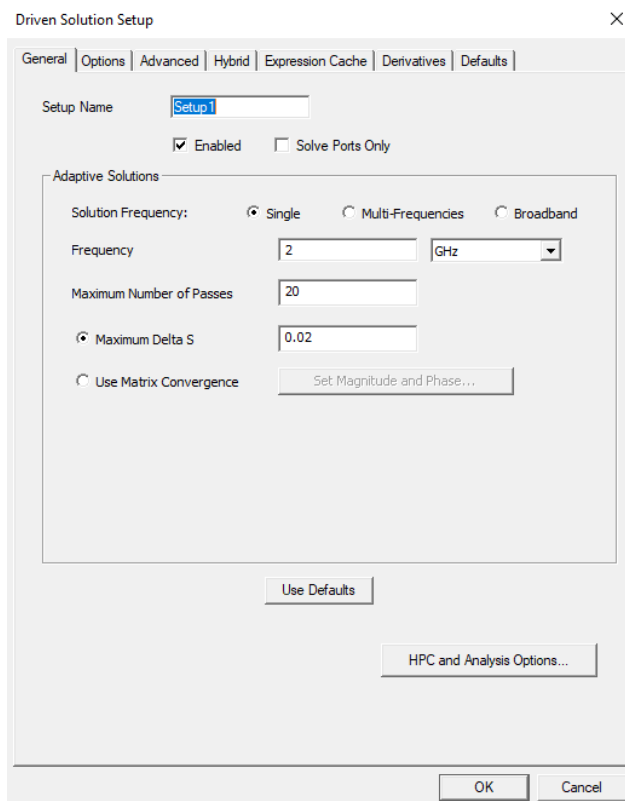


Figure 22 Screenshot of Simulation Setup

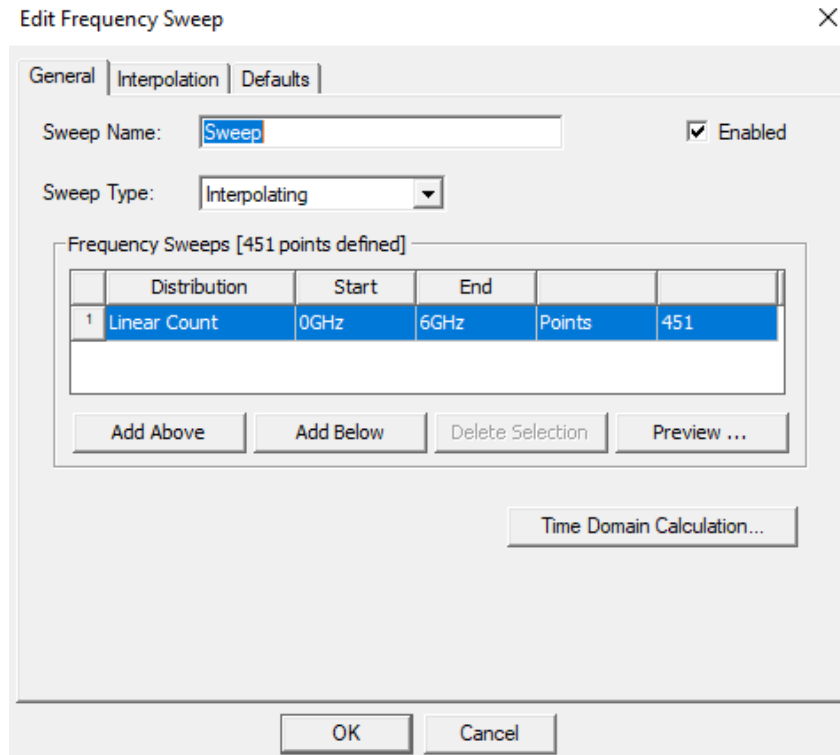


Figure 23 Adding Frequency Sweep

3.4.1 Simulated Results of the Three Types of the CB-CPW LPF

After creating models in HFSS, corresponding simulated results are generated. As examples, the most three representative optimized designs are chosen as type 1 CB-CPW LPF using TRRA, type 2 CB-CPW LPF using PSO, type 3 CB-CPW LPF using GA. Figure 24, 25 and 26 show their corresponding simulated results as follows.

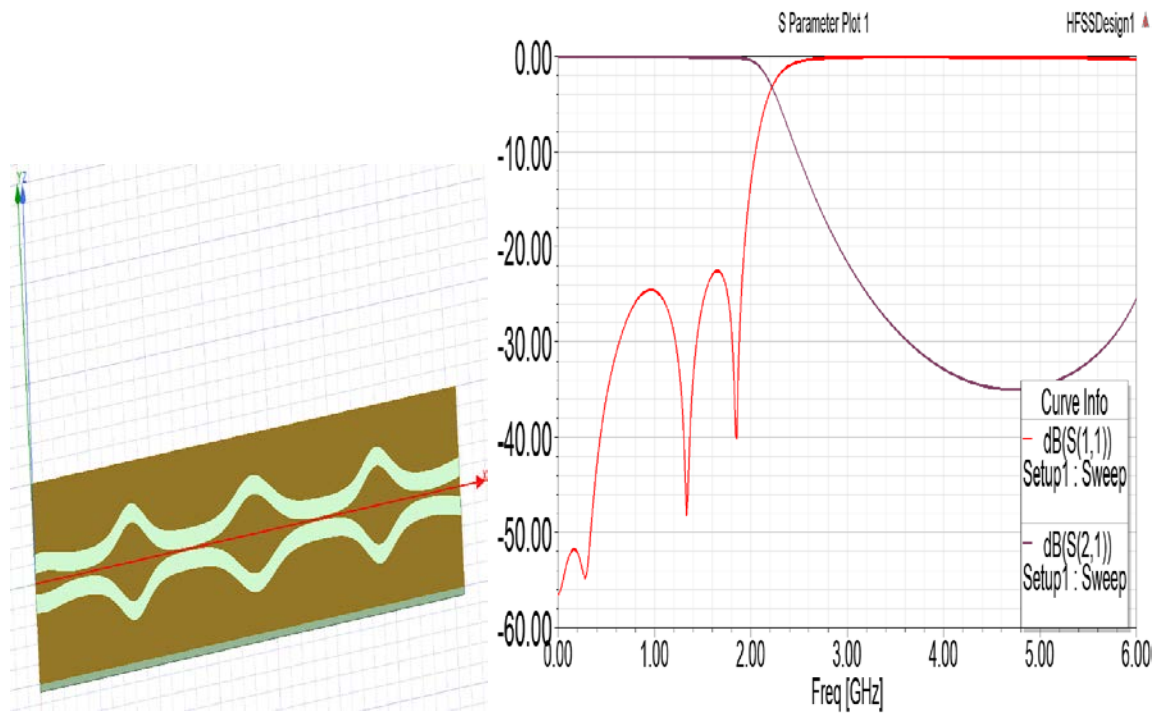


Figure 24 Type 1 CB-CPW LPF and Corresponding Simulated Results

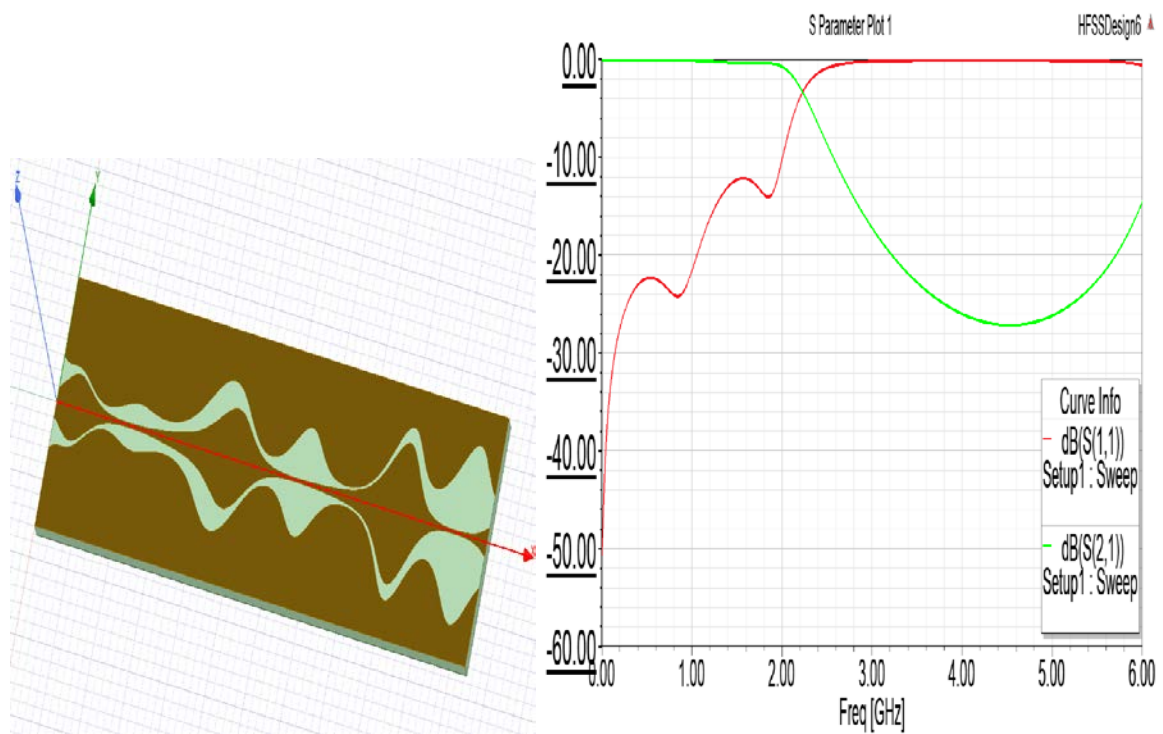


Figure 25 Type 2 CB-CPW LPF and Corresponding Simulated Results

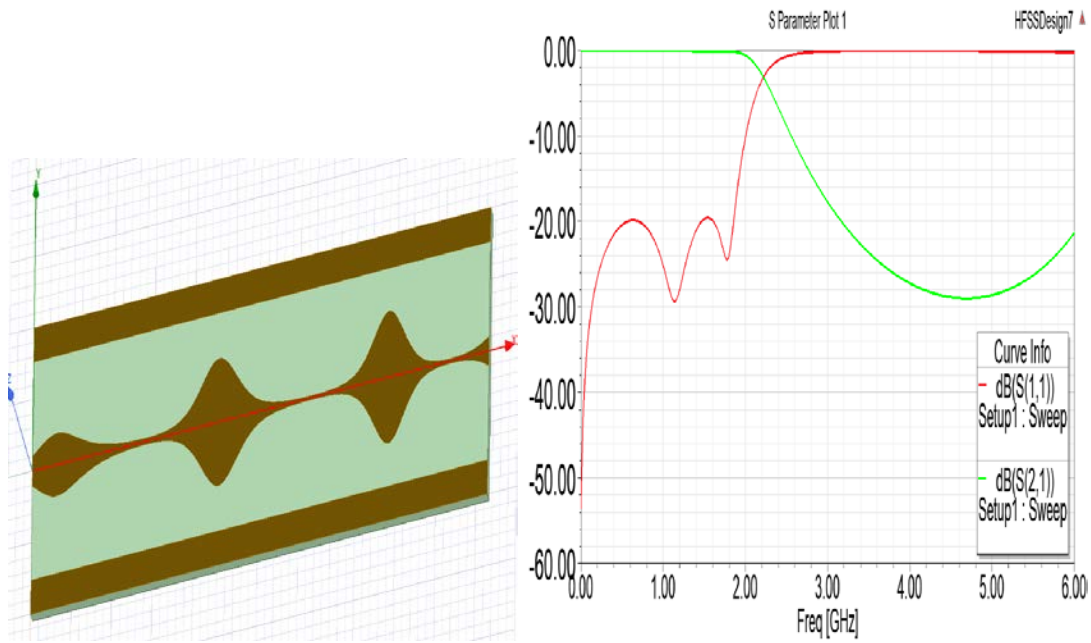


Figure 26 Type 3 CB-CPW LPF and Corresponding Simulated Results

In conclusion, all proposed designs are validated to achieve the desired electrical characteristics and can be functionally used as LPF.

3.4.2 Comparison between Analytical and Simulated Results

For the purposes of validity check, the simulated results obtained above are plotted with corresponding analytical results as shown in Figure 27, 28 and 29.

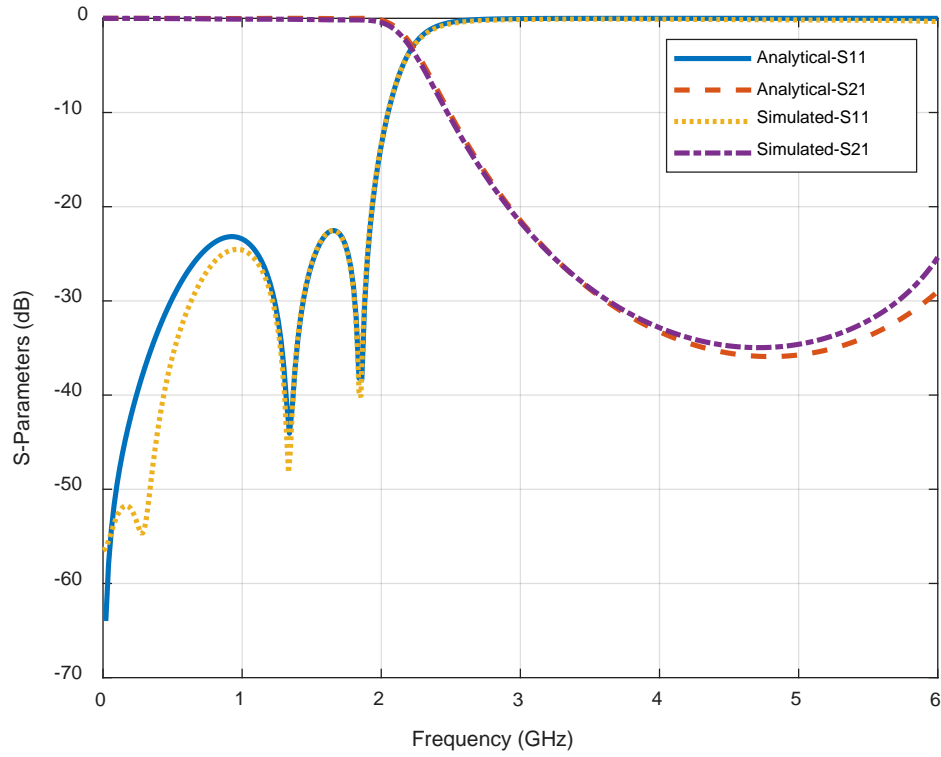


Figure 27 Comparison between Analytical and Simulated Results on Type 1

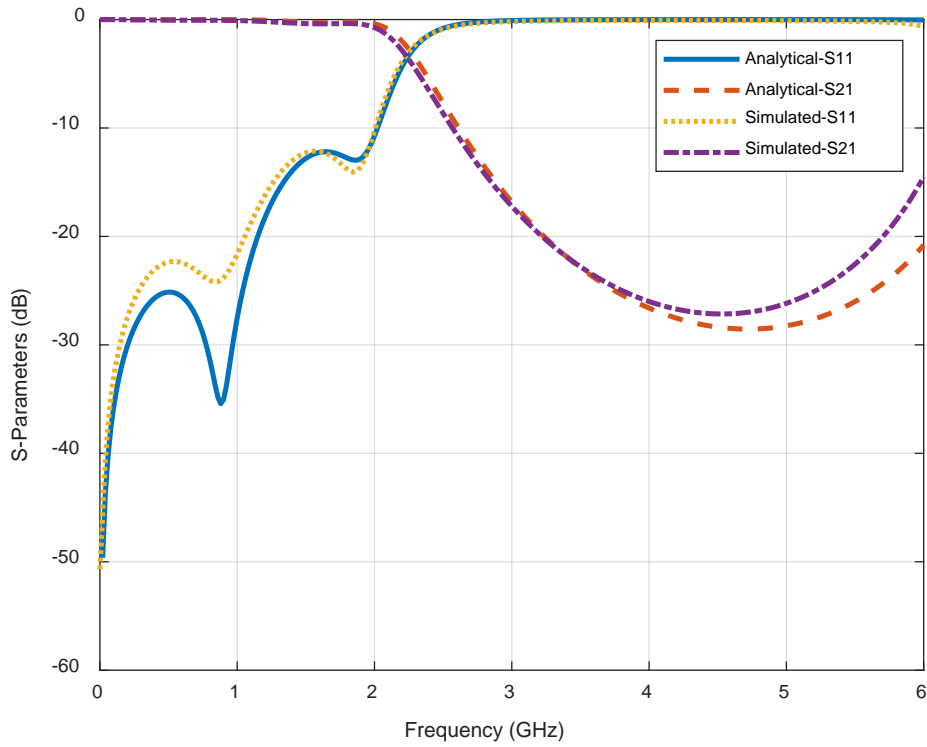


Figure 28 Comparison between Analytical and Simulated Results on Type 2

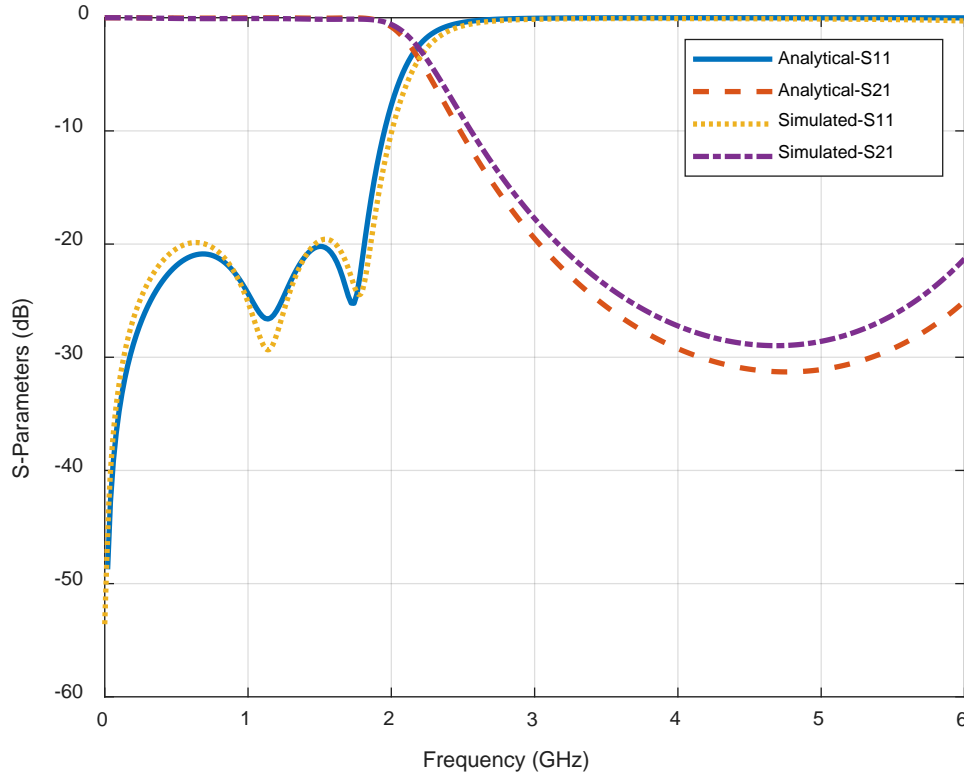


Figure 29 Comparison between Analytical and Simulated Results on Type 3

To sum up, all simulated results have a good agreement with analytical results. Therefore, it is proved that our proposed designs are successfully obtained from the developed methodology and all CB-CPW LPFs can be fabricated and utilized in practice.

3.4.3 Design of the Conventional Stepped-impedance CB-CPW LPF

To make comparison between the proposed CB-CPW LPF and conventional stepped-impedance CB-CPW LPF designs, the design of conventional stepped-impedance CB-CPW LPF is presented. A relatively easy way to implement low pass filters in CB-CPW is to use alternating sections of very high and very low characteristics impedance lines. Such filters are usually referred to as stepped-impedance, or hi-Z, low-Z filters [15]. In this section, a stepped-impedance CB-CPW LPF meeting same conditions as our proposed non-uniform CB-CPW LPF is designed. Specifically, the cutoff frequency is set to 2 GHz, and it is desired to have more than 20 dB insertion loss at 3 GHz. The filter impedance is 50Ω ; the highest practical line impedance is set to 136Ω , and the lowest is 14Ω as before. Also, this filter is implemented with the same substrate,

Rogers RO4003 substrate having 0.813mm thickness H , with a relative permittivity ϵ_r of 3.55 and a dielectric loss tangent $\tan \delta$ of 0.0027.

To have a maximally flat response at the desired frequency, it is found out that the stepped-impedance CB-CPW LPF has to be at least 6th order. The required electrical line lengths, βl_i , along with the physical CB-CPW line widths W_i , and lengths, l_i , are obtained in Table 7 as below (S is constant, set to 2 mm):

Table 7 Relevant Parameters of the Designed Stepped-Impedance CB-CPW LPF

Section	$Z_i = Z_l \text{ or } Z_h (\Omega)$	βl_i (rad)	W_i (mm)	l_i (mm)
1	13.84	0.1431	10	1.9065
2	136.25	0.5189	0.2	7.8129
3	13.84	0.5348	10	7.125
4	136.25	0.7090	0.2	10.6752
5	13.84	0.3914	10	5.2145
6	136.25	0.1897	0.2	2.8562

After getting the structure of designed stepped-impedance CB-CPW LPF, the 2D schematic model can be set up by choosing desired components and substrate in HFSS as circuit design as shown in Figure 30 and Figure 31.

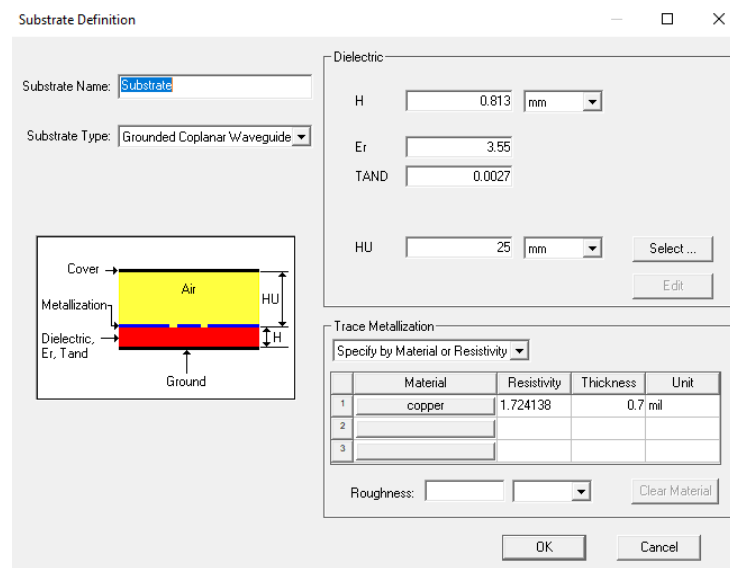


Figure 30 Setting up Substrate

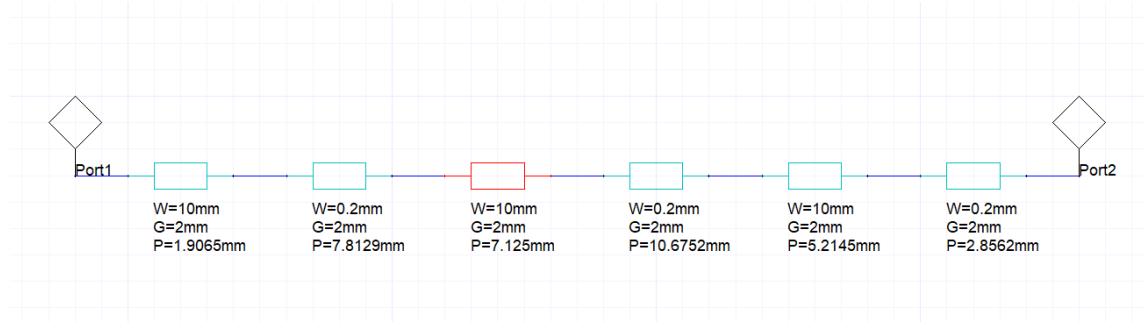


Figure 31 Schematic of the Designed Stepped-Impedance CB-CPW LPF Circuit

Figure 32 shows the simulation results of designed stepped-impedance CB-CPW LPF circuit. The result demonstrates the validity of the design. The cutoff frequency is 2 GHz and insertion loss is -20 dB at 3 GHz as desired. Moreover, the 3D geometry is inserted to HFSS and being simulated. The simulated result shown in Figure 33 is more accurate and reliable, and it accords with the simulated result of 2D circuit and predefined requirements.

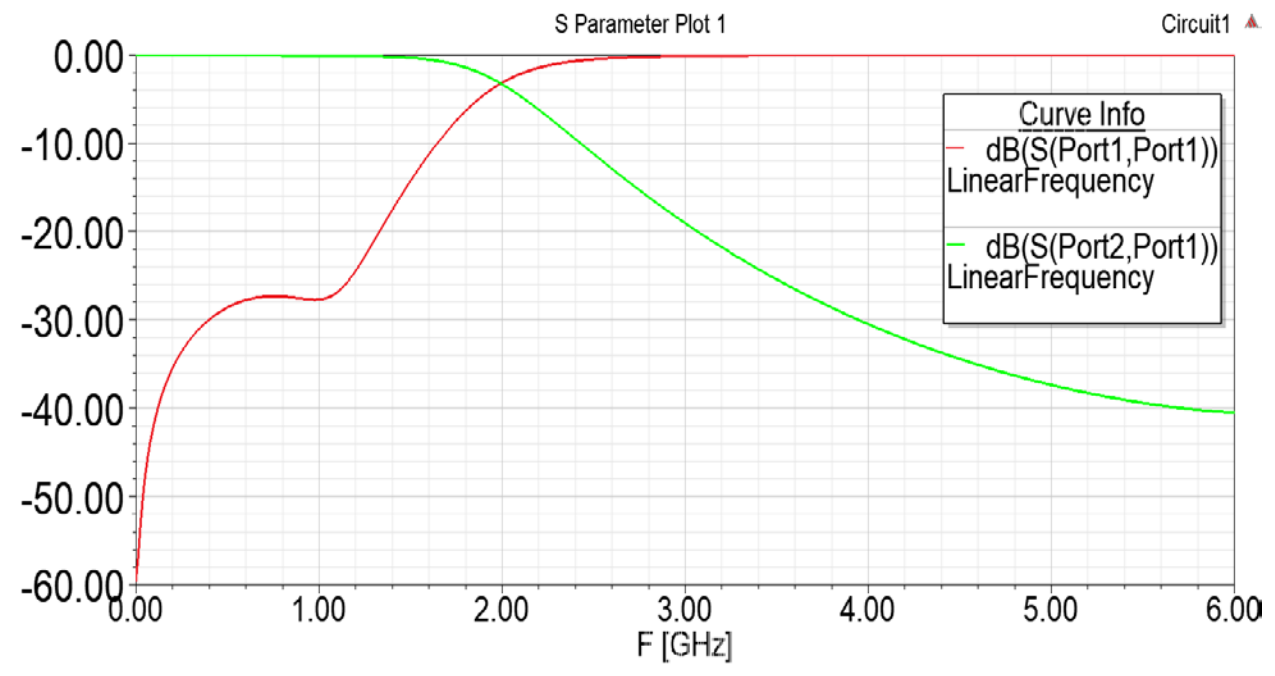


Figure 32 Simulated Results of 2D Designed Circuit

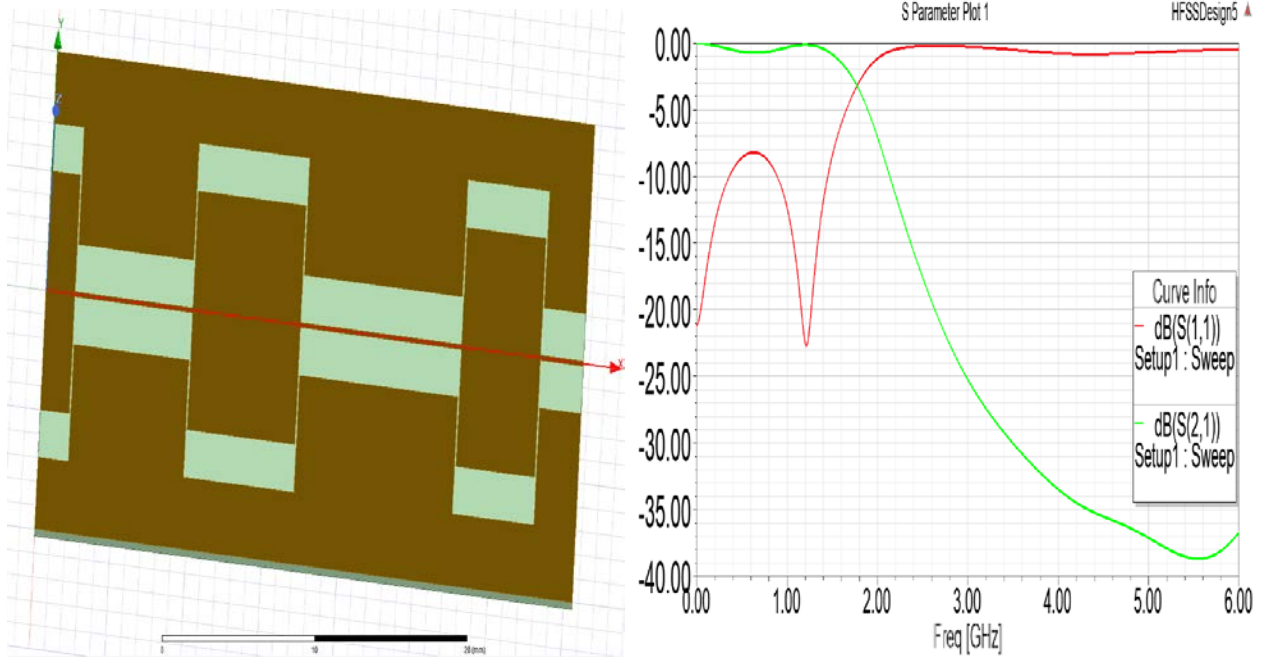


Figure 33 Designed Stepped-Impedance CB-CPW LPF and Corresponding Simulated Result

3.4.4 Comparison between Conventional and Proposed Non-uniform CB-CPW LPFs

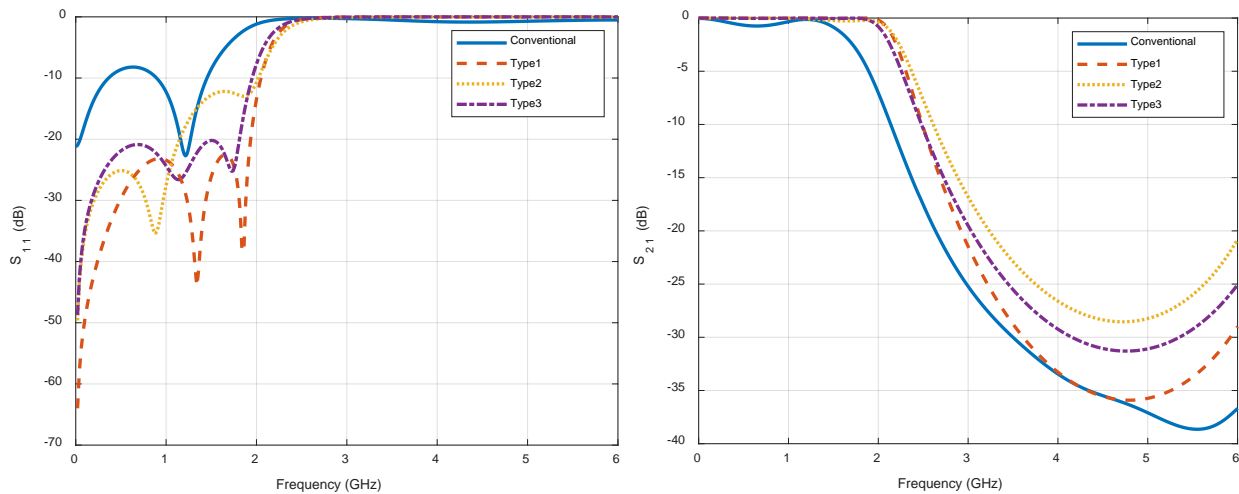


Figure 34 Simulated Results between Three Types of Designs and Conventional CB-CPW LPF

Figure 34 visualizes the advantages of our proposed non-uniform CB-CPW LPFs. All types of designs have better performance over conventional stepped-impedance CB-CPW LPF at [0, 3] GHz. It is because the proposed non-uniform CB-CPW LPF has less discontinuity which causes loss in the high/low transitions as compared to a conventional stepped-impedance LPF [59]. On

the other hand, transmission parameter S_{21} of conventional one starts to drop at unwanted 1.5 GHz. The curve of S_{21} is acceptable that even non-uniform CBCPW LPFs are approximately 5 dB higher than conventional one. As a matter of fact, the conventional stepped-impedance CBCPW LPFs only have benefits over non-uniform ones in size. The conventional CB-CPW LPF is designed with the length around of 36 mm; whereas proposed ones are about 70 mm long.

CHAPTER 4. PROPOSED CONVENTIONAL CPW-BASED LPF

Besides CB-CPW-based LPW designs, the conventional CPW-based LPF is presented as well [60]. All the predefined parameters are same as the ones set for CB-CPW-based LPF designs. However, in this design, only type 1 structure is considered and only TRRA is taken into account. In this case, reference and gap widths are set to $W_{ref} = 2$ mm and $S = 0.2$ mm to meet termination impedance as 50Ω . Also, the cutoff frequency is set to 3.5 GHz instead and the total length of the transmission line d is fixed to 100 mm.

4.1 Analytical Results

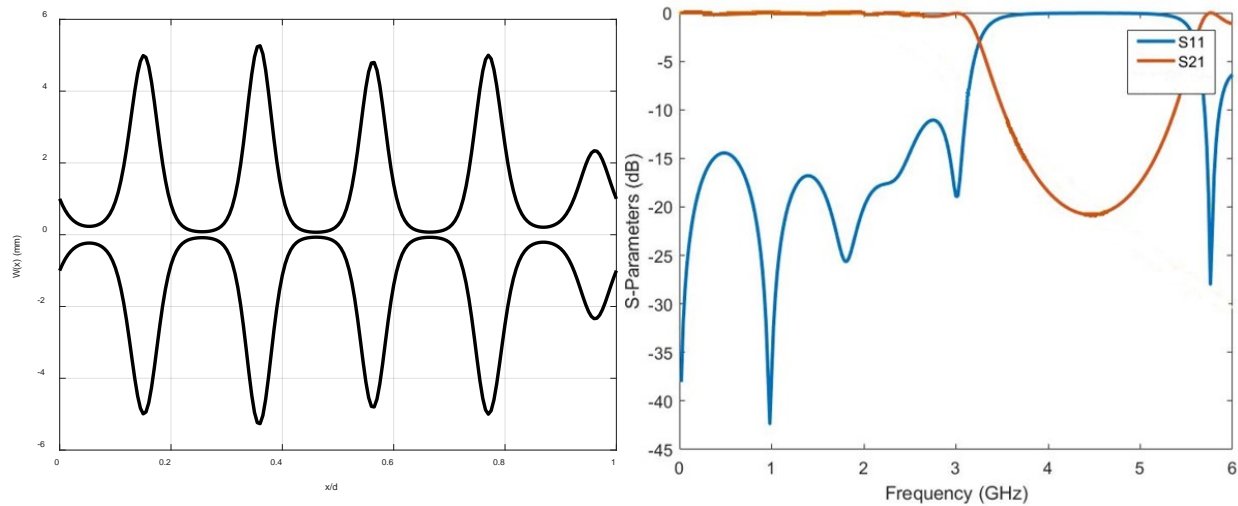


Figure 35 Optimized CPW LPF Width Profile with Corresponding Analytical Response

Figure 35 shows the resulting optimized width profile of the non-uniform trace, which is in a good agreement with the predefined constraints. Within the passband, the input port matching parameter, S_{11} , is below -10 dB, and the transmission parameter, S_{21} , is around -0.2 dB. At the cutoff frequency, S_{21} gradually decreases to almost -20 dB.

4.2 Simulated Results

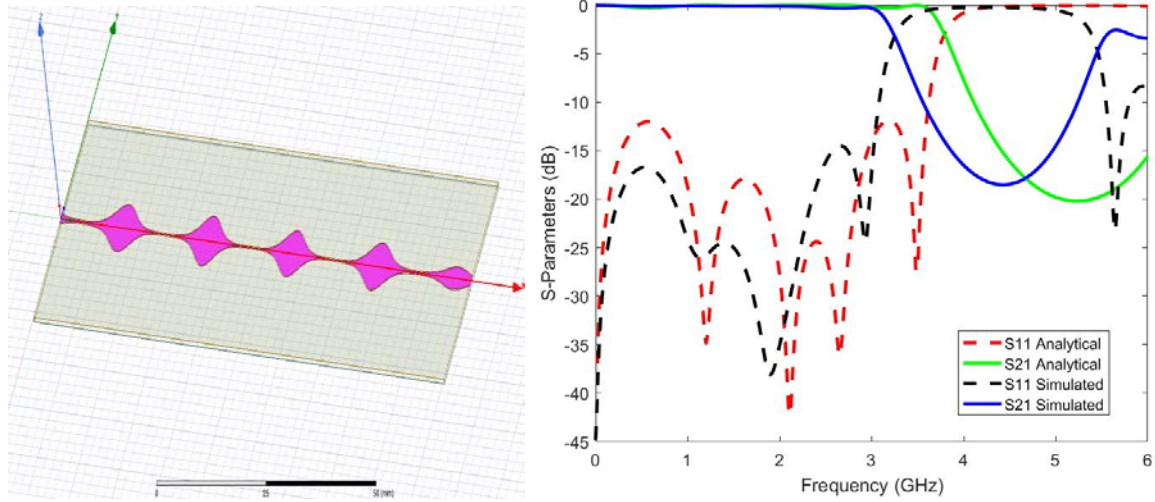


Figure 36 Optimized CPW LPF and Corresponding Simulated Results

Analytical and simulated results of the S -parameters are shown in Figure 36. The discrepancies between the analytical and simulated results are due to different types of losses, (e.g., conductor, dielectric, and radiation losses). Hence, the first proposed type of CPW LPF using TRRA satisfied with predefined conditions is gathered.

CHAPTER 5. CONCLUSIONS

The proposed systematic methodology is introduced and tested to achieve a CB-CPW LPF with arbitrary predefined conditions. The uniform width of the conventional CB-CPW structure is replaced by a width-varying transmission line by modeling in a truncated Fourier series taking into account three structural types. Mathematical and theoretical analysis is established, optimized, and the resulting filter is simulated considering three investigated optimization techniques. Analytical and simulated results are in a good agreement and advantages are been addressed by making comparisons with conventional stepped-impedance LPF. LPFs with 2 GHz cutoff frequencies show a matching better than -20 dB and transmission parameter achieves -30 dB in stop band.

Furthermore, a CPW LPF with 3.5 GHz cutoff frequency shows a matching better than -10 dB and transmission parameter achieves -20 dB in stop band. This ongoing research aims to further enhance the electrical response at the stopband by applying optimization techniques/approximations to tackle the high nonlinearity degree of the CPW structures and design equations.

REFERENCES

- [1] Wen, C.: 'Coplanar waveguide: a surface strip transmission line suitable for nonreciprocal gyromagnetic device applications' *IEEE Trans. Microw. Theory and Techn.*, 1969, 17, (12), pp. 1087-1090.
- [2] Ghione, G and Naldi, C.: 'Parameters of coplanar waveguides with lower ground plane' *Electron. Lett.*, 1983, 19, (18), pp. 734-735.
- [3] Simons, R.: 'Coplanar waveguide circuits components and systems' Wiley, 2001.
- [4] Ghione, G and Naldi, C.: 'Analytical formulas for coplanar line in hybrid and monolithic MICs' *Electron. Lett.*, 1984, 20, (4), pp. 179-181.
- [5] Hudson, S., Pozar, D.: 'Grounded coplanar waveguide-fed aperture-coupled cavity-backed microstrip antenna' *Electronics Lett.*, 2000, 36, (12), pp. 1003-1005.
- [6] Tien, C.-C., Tzuang, C.-K. C., Peng, S. T., Chang, C.-C.: 'Transmission characteristics of finite-width conductor-backed coplanar waveguide' 1993, *IEEE Trans. Microw. Theory and Techn.*, 41, (9), pp. 1616-1624.
- [7] Yu, M., Vahldieck, R., Huang, J.: 'Comparing coax launcher and wafer probe excitation for 10 mil conductor backed CPW with via holes and airbridges' *IEEE MTT-S Int. Microw. Symp. Dig.*, 1993, 2, pp. 705-708.
- [8] Haydl, W. H.: 'Resonance phenomena and power loss in conductor-backed coplanar structures' *IEEE Microw. Guided Wave Lett.*, 2000, 10, (12), pp. 514-516.
- [9] Haydl, W. H.: 'On the use of vias in conductor-backed coplanar circuits' *IEEE Trans. Microw. Theory Techn.*, 2002, 50, (6), pp. 1571-1577.
- [10] Das, N. K.: 'Methods of suppression or avoidance of parallel-plate power leakage from conductor-backed transmission lines' *IEEE Trans. Microw. Theory Techn.*, 1996, 44, (2), pp. 169-181.
- [11] Pucel, R. A.: 'Design considerations for monolithic microwave circuits' *IEEE Trans. Microw. Theory and Techn.*, 1981, 29, (6), pp. 513-534.
- [12] Shih, Y. C., Itoh, T.: 'Analysis of conductor-backed coplanar waveguide' *Electronics Lett.*, 1982, 18, (12), pp. 538-540.

- [13] Sain, A., Melde, K. L.: 'Impact of ground via placement in grounded coplanar waveguide interconnect' *IEEE Transactions on Components, Packaging and Manufacturing Technology*, 2016, 6, (1), pp. 136-144.
- [14] Amrani, S., Rodriguez-Berral, R. and Mesa, F.: 'Effects of the bottom ground plate on coplanar waveguide structures' *IET Microw. Anten. Propag.*, 2013, 7, (8), pp. 708-713.
- [15] K. C Jayakrishnan, Nair, S. Bhuvana, S. K Menon.: 'Analysis of Metamaterial based band pass filter' 3rd International Conference on Signal Processing and Integrated Networks, 2016.
- [16] R. Azaro, M. Donelli, A. Massa, F. De Natale, E. Zeni.: 'Synthesis of a prefractal dual-band monopolar antenna for GPS applications' *IEEE Antennas and Wireless Propagation Letters*, 2006, 5, (1), pp. 361-364.
- [17] D. M. Vijayan, A.M, S. K. Menon.: 'Patch loaded CPW fed monopole antenna' 3rd International Conference on Signal Processing and Integrated Networks, 2016.
- [18] M. S. Sooraj Subramanian, K. V. Siddharth, S. N. Abhinav, V. V. Arthi, K. S. Praveen, R. Jayavarshini, G. A. Shanmugha Sundaram.: 'Design of dual log-spiral metamaterial resonator for X-band applications' 2012 International Conference on Computing Communication and Applications ICCCA 2012, 2012.
- [19] S. Sarathkrishna, K. Balamurugan, M. Nirmala Devi, M. Jayakumar.: 'Design and analysis of GaN HEMT based LNA with CPW matching' 2014 Eleventh International Conference on Wireless and Optical Communications Networks (WOCN), 2014.
- [20] Amit Ghosh, Rudra Vaswata Roy Choudhury.: 'Design and Fabrication of a S band Multi-stub CPW Band Pass Filter for improved Filter Characteristics' International Conference on Microwave and Photonics (ICMAP), 11-13 Dec. 2015.
- [21] Bingzheng Yang, Huizhen Qian, Xun Luo.: 'Compact CPW Bandpass Filter with Ultra-Wide Stopband using Slow-Wave Structure' *IEEE International Workshop on Electromagnetics: Applications and Student Innovation Competition (iWEM)*, 2016.
- [22] Elif Gunturkun, Adnan Gorur, Ceyhun Karpuz.: 'A novel bandstop filter design with CPW-fed microstrip square loop resonator' 43rd European Microwave Conference, 2013.
- [23] S. Preradovic, N. C. Karmakar, *Multiresonator-Based Chipless RFID - Barcode of the future*, Springer, 2012.

- [24] Hong, H.S., Shaman, H.: "An optimum ultra-wideband microstrip filter' Microwave and Optical Technology Letters, 2005, 47, pp. 230-233.
- [25] Tsujiguchi, T., Matsumoto, H., Nishikawa, T.: 'A miniaturized double-surface CPW bandpass filter improved spurious responses' IEEE Trans. on Microw. Theory and Techn., 2001, 49, (5), pp. 879-885.
- [26] Zhang, H., Chen, K.J.: "Compact bandpass filters using slow-wave coplanar waveguide tri-section stepped-impedance resonators' IEEE Microwave Conference Proceedings, 2006.
- [27] Chen, Y.-C., Lin, Y.-S.: 'Coplanar waveguide bandpass filter with hollow-t shaped transmission-line resonator for multiple spurious suppression' IEEE Wireless and Microwave Technology Conference (WAMICON), 2013.
- [28] Yang, B., Qian, H., Luo, X.: 'Compact CPW bandpass filter with ultra-wide stopband using slow-wave structure' IEEE Conference Publications, 2016.
- [29] Kim, J., Cho, C.S., Lee, J.W.: 'CPW bandstop filter using slot-type SRRs' Electronics Letters, 2005, 41, (24), pp. 1333-1334.
- [30] Kim, J.Y. and Lee, H. Y.: 'Wideband and compact Bandstop filter structure using double-plane superposition' IEEE Microwave Guided Wave Lett., 2003, 13, (7), pp. 279-280.
- [31] Zhang, X.J., Liu, A.Q., Karim, M.F., Yu, A.B., Shen, Z.X.: 'MEMS-based photonic bandgap (PBG) band-stop filter' 2004 IEEE MTT-SInt. Microwave Symp. Dig., 2004, 3, pp. 1463-1466.
- [32] Sor, J., Qian, Y. and Itoh, T.: 'Miniature low-loss CPW periodic structures for filter applications' IEEE Trans. Microw. Theory and Techn., 2001, 49, (12), pp. 2336-2341.
- [33] No, J.W. and H.-Yong, H.: 'A design of cascaded CPW low-pass filter with broad stopband' IEEE Microw. Wireless Compon. Lett., 2007, 17, (6), pp. 427-429.
- [34] Kanamaluru, S., M. Yi, L. and Kai, C.: 'Coplanar waveguide low-pass filter using open circuit stubs' Microw. Opt. Technol. Letters, 1993, 6, (12), pp. 715-717.
- [35] Hao-Jia, L., et al.: 'A wide stopband CPW low pass filter using quarter wavelength stepped impedance resonators' 2010 International Conference on Microwave and Millimeter Wave Technology.

- [36] Miguel, D.S., Jordi, B. and Ferran, M.: 'Compact elliptic-function coplanar waveguide low-Pass filters using backside metallic patterns' *IEEE Microw. Wireless Compon. Lett.*, 2010, 20, (11), pp. 601-603.
- [37] Chia-Cheng, H., et al.: 'A coplanar waveguide bandwidth-tunable lowpass filter with broadband rejection' *IEEE Microw. Wireless Compon. Lett.*, 2013, 23, (3), pp. 134-136.
- [38] Hong-Teuk, K., et al.: 'A new micromachined overlay CPW structure with low attenuation over wide impedance ranges and its application to low-Pass filters' *IEEE Trans. Microw. Theory and Techn.*, 2001, 49, (9), pp. 1634–1639.
- [39] Aznar, F., et al.: 'Elliptic-function CPW low-pass filters implemented by means of open complementary split ring resonators (OCSRRs)' *IEEE Microw. Wireless Compon. Lett.*, 2009, 19, (11), pp. 689–691.
- [40] Kaddour, D., et al.: 'A compact and selective low-Pass filter with reduced spurious responses, based on CPW tapered periodic structures' *IEEE Trans. Microw. Theory and Techn.*, 2006, 54, (6), pp. 2367–2375.
- [41] Gauthier, G.P. Katehi, L.P., Rebeiz, G.M.: 'W-band finite ground coplanar waveguide (FGCPW) to microstrip line transition' *IEEE MTT-S Int. Dig.*, 1998, 1, pp. 107.
- [42] Safwata, A.M.E., Zaki, K.A., Johnson, W., Lee, C.H.: 'Novel design for coplanar waveguide to microstrip transition' *IEEE MTT-S Int. Dig.*, 2001, 2, pp. 607.
- [43] Lin, T.H.: 'Via-free broadband microstrip to CPW transition' *Electron. Lett.*, 37, (15), pp. 960.
- [44] Kim, Y.G., et al.: 'An ultra-wideband microstrip-to-CPW transition' *IEEE MTT-S Int. Dig.*, 2008, pp. 1079.
- [45] Zhou, Z., Melde, K.L.: 'Development of a broadband coplanar waveguide-to-microstrip transition with vias' *IEEE Trans. Adv. Packag.*, 2008, 31, (4), pp. 861.
- [46] Baik, J.-W., Lee, T.H., Kim, Y.-S.: 'UWB bandpass filter using microstrip-to-CPW transition with broadband balun' *IEEE Microwave and Wireless Component Letters*, 2007, 17, (12), pp. 846-848.
- [47] Kuo, T., Lin, S., Chen, C.H.: 'Compact ultra-wideband bandpass filters using composite microstrip-coplanar-waveguide structure' *IEEE Trans. Microw. Theory Tech.*, 2006, 54, (10), pp. 3772-3778.

- [48] Abbosh, A., Bialkowski, M., Ibrahim, S.: 'Ultra-wideband bandpass filters using broadside-coupled microstrip-coplanar waveguide' *IET Microw. Antennas Propag.*, 2011, 5, (7), pp. 764-770.
- [49] Pozar, D.: 'Microwave engineering' Wiley, 4th edn., 2011.
- [50] Simons, R.: 'Coplanar waveguide circuits components and systems' Wiley-IEEE Press, 1st edn., 2001.
- [51] Hilberg, W.: 'From approximations to exact relations for characteristic impedances, *IEEE Trans. Microw. Theory and Techn.*, 1969, MTT-17, (5), pp.259-265.
- [52] Al Shamaileh, K., Dib, N., Devabhaktuni, V.: 'Impedance-varying broadband 90° branch-line coupler with arbitrary coupling levels and higher order harmonic suppression' *IEEE Trans. Compon. Pack. Manufac. Technol.*, 2015, 5, (10), pp. 1507-1515.
- [53] Khalaj-Amirhosseini, M. and A Akbarzadeh-Jahromi, S.: 'To optimally design microstrip nonuniform transmission lines as lowpass filters' *Journal of Telecommunications*, 2010, 2, (2), May 2010.
- [54] Li, Y.: 'Centering trust region, reflective techniques for nonlinear minimization subject to bounds, Dept. Comput. Sci., Cornell Univ., Ithaca, NY, USA, Tech. Rep. 93-1385, 1993.
- [55] Cui C., Li, W., Ye, X., Shi, X.: 'Hybrid genetic algorithm and modified iterative Fourier transform algorithm for large thinned array array synthesis' *IEEE Anten. Wireless Propag. Lett.*, 2017, 16, pp. 2150-2154.
- [56] Chou, H.-T., Cheng, D.-Y.: 'Beam-pattern calibration in arealistic system of phased-array antennas via the implementation of a genetic algorithm with a measurement system' *IEEE Trans. Anten. Propag.*, 2017, 65, (2), pp. 593-601.
- [57] Li, Y.-L., et al.: 'An improved PSO algorithm and its application to UWB antenna design' *IEEE Trans. Anten. Propag.*, 2013, 12, pp. 1236-1239.
- [58] 'ANSYS Electronics Desktop – HFSS, www.ansys.com/products/electronics/ansys-electronics-desktop, accessed 10 January 2018.
- [59] Al Shamaileh, K., Dib, N., Abushamleh, S.: 'Width-varying conductor-backed coplanar waveguide-based low-pass filter with a constant signal trace to adjacent grounds separation' *IET Microw. Antennas and Propag.*, 2019, 13, (3), pp. 386-390.

- [60] Li, Q., Al Shamaileh, K., Devabhaktuni, V.: ‘ Coplanar waveguide-based lowpass filters with non-uniform signal trace and ground planes’ 2018 International Applied Computational Electromagnetics Society Symposium (ACES), May 2018.